

AD-A112 812

LINCOM CORP PASADENA CA
BIT SYNCHRONIZATION WITH CROSS SPECTRUM SYNCHRONIZATION LOOP. A--ETC(U)
OCT 81 R A MAAG, W C LINDSEY, C M CHIE

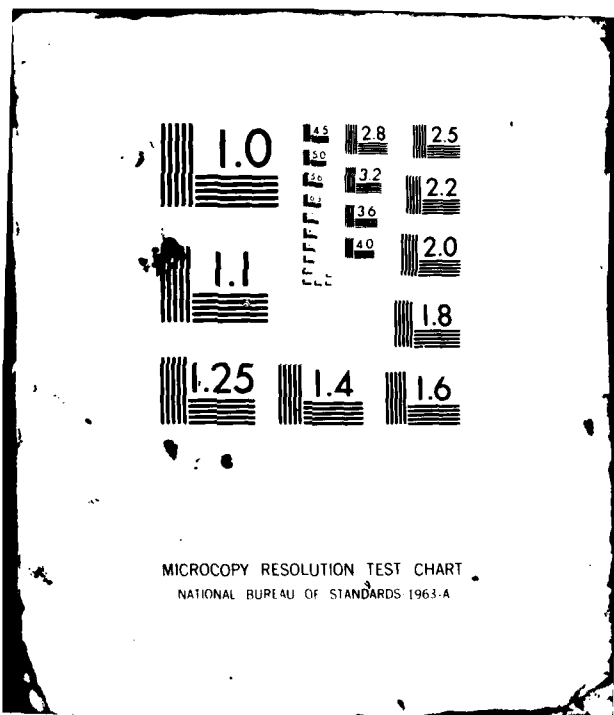
F/6 9/2
N00014-81-C-2338
NL

UNCLASSIFIED

1 1
0 0

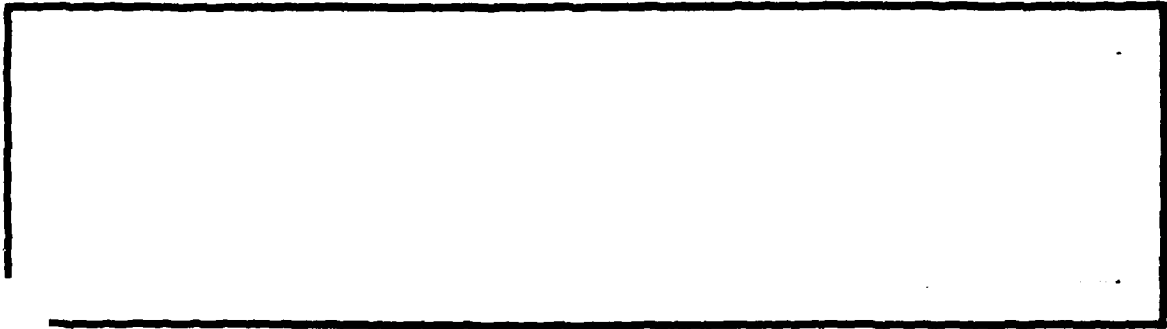
| | | | | | | | | | | | | | | | | | | | | |
|--|--|--|--|--|--|--|--|--|--|--|--|--|--|--|--|--|--|--|--|--|
| | | | | | | | | | | | | | | | | | | | | |
| | | | | | | | | | | | | | | | | | | | | |
| | | | | | | | | | | | | | | | | | | | | |
| | | | | | | | | | | | | | | | | | | | | |

END
DATE
FILMED
4 82
DTIC



MICROCOPY RESOLUTION TEST CHART
NATIONAL BUREAU OF STANDARDS 1963-A

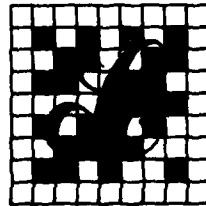
12



ADA 112812

DTIC FILE COPY

DTIC
MAR 30 1982
H



DISTRIBUTION STATEMENT A
Approved for public release;
Distribution Unlimited

Lincom Corporation

P.O. Box 2793D, Pasadena, Calif. 91105

82 03 09 098

12

ATTACHMENT III

BIT SYNCHRONIZATION WITH CROSS SPECTRUM SYNCHRONIZATION LOOP

PREPARED FOR

NAVAL RESEARCH LABORATORY
WASHINGTON, D.C. 20375

TECHNICAL MONITOR: MR. MORT FRANK

CONTRACT NO. N00014-81-C-2338
TASK 3

PROGRAM DIRECTOR:

R. A. MAAG

PREPARED BY

W. C. LINDSEY
C. M. CHIE
C. S. TSANG

LINCOM CORPORATION
P.O. BOX 2793D
PASADENA, CA 91105

DTIC
SELECTED
MAR 30 1982
H

DISTRIBUTION STATEMENT A
Approved for public release;
Distribution Unlimited

OCTOBER, 1981

TR-1082-0881a

TABLE OF CONTENTS

| | PAGE |
|--|------|
| Summary | 1 |
| 1. INTRODUCTION | 2 |
| 2. SYSTEM MODEL OF CSSL | 2 |
| 3. PERFORMANCE ANALYSIS OF CSSL | 4 |
| 4. NUMERICAL RESULTS | 13 |
| 5. PERFORMANCE COMPARISON BETWEEN CSSL AND DTL | 21 |
| 6. SUMMARY | 31 |
| APPENDIX A | 35 |
| APPENDIX B | 37 |
| APPENDIX C | 39 |
| REFERENCES | 45 |

DTIC
COPY
INSPECTED
2

| | |
|--------------------|-------------------------------------|
| Accession For | |
| CRA&I | <input checked="" type="checkbox"/> |
| T&B | <input type="checkbox"/> |
| Un. Prod | <input type="checkbox"/> |
| Justification | |
| By _____ | |
| Distribution/ | |
| Availability Codes | |
| Dist | Special |
| A | |

LIST OF FIGURES

| | PAGE |
|---|------|
| Figure 1. Cross-Spectrum Symbol Synchronizer. | 3 |
| Figure 2. Normalized Harmonic Power Versus Filter Time Bandwidth Product. | 14 |
| Figure 3. Normalized Harmonic Power vs. Filter Time Bandwidth. | 15 |
| Figure 4. $ C_n ^2$ versus f_0T . | 16 |
| Figure 5. S_L vs f_0T for Various α , Biphase Format. | 17 |
| Figure 6. S_L vs f_0T for Various α , Biphase Format. | 18 |
| Figure 7. S_L vs f_0T for Various α , NRZ Format. | 19 |
| Figure 8. S_L vs f_0T for Biphase and Different Filters. | 20 |
| Figure 9. S_L vs f_0T for NRZ and Different Filters. | 22 |
| Figure 10. S_L vs R_s for Biphase and Different Filters. | 23 |
| Figure 11. S_L vs R_s for NRZ and Different Filters. | 24 |
| Figure 12. S_L vs p_t for Biphase and Various R_s , $R_s=5$ dB. | 25 |
| Figure 13. S_L vs p_t for Biphase and Various R_s , $R_s=15$ dB. | 26 |
| Figure 14. S_L vs p_t for Biphase and Various R_s , $R_s=-5$ dB. | 27 |
| Figure 15. S_L vs p_t for NRZ and Various R_s . | 28 |
| Figure 16. Clock Jitter vs S_L . | 29 |
| Figure 17. \bar{S}/W_L vs S_L for Sinusoidal PLL. | 30 |
| Figure 18. S_L vs R_s for DTTL, NRZ Format. | 32 |
| Figure 19. S_L vs R_s for DTTL Bi-Phase Format. | 33 |
| Figure C.1. Bi-Phase Signal $S(t)$ for Different Data Patterns. | 40 |

LIST OF TABLES

| | PAGE |
|---|------|
| Table C.1. Definition of $x_{(i)}$ and $y_{(i)}$. | 41 |
| Table C.2. Values of x_k, y_k for Different Data Patterns, Unshifted Case. | 41 |
| Table C.3. Values of x_k, y_k for Different Data Patterns, Shifted Case. | 42 |

BIT SYNCHRONIZATION WITH CROSS SPECTRUM SYNCHRONIZATION LOOP

T. S. Tsang
C. M. Chie
W. C. Lindsey

LinCom Corporation
P.O. Box 2793D
Pasadena, CA 91105

Summary

- study seeks

The purpose of this report is two-fold: (a) to identify the optimal analog technique for implementing a bit synchronizer for wide-band data channels, and (b) to compare, in detail, the performance of the analog bit synchronizer with the optimal digital implementation exemplified by the DTTL already built and tested. For biphasic data, it is shown that the optimal analog implementation based upon the cross-spectrum principle is a delay-and-multiply circuit followed by a conventional CW loop. The optimal delay is about one-quarter of the bit duration. For a 12.5 Mbps data stream, it is roughly 20 ns. The IF filter in front of the delay-and-multiply nonlinearity is immaterial as long as the BT product exceeds three approximately.

By the Data Transfer Tracking Loop

When compared to the DTTL, the performance of the analog loop is roughly equivalent to a DTTL with a 50% error arm window. It outperforms a full-window DTTL by roughly 3 dB in terms of jitter yet gives inferior acquisition performance. On the other hand, a DTTL with a quarter-window outperforms the analog loop by roughly the same amount.

It therefore appears that both the analog and digital bit synchronizer performs equally well. The selection of one over the other must be based on other criteria such as sensitivity to environmental variations, biases, stability and perhaps packaging ease.

1. INTRODUCTION

Bit synchronization [1,2] is an important and well-established area in communication theory; however, a detailed analysis which compares analog loop implementations with that of digital implementations has not been fully performed. Recently, a detailed analysis of an old bit synchronizer, viz., the Filter and Square Bit Synchronizer Loop (FSTL) was done by J. K. Holmes [3]. A modification of the FSTL was introduced by McCallister and Simon [4] which used a delay and multiply circuit instead of the squaring circuit. This configuration, the Cross-Spectrum Symbol Synchronization (CSSL), shown in Fig. 1, has been demonstrated to have a better performance than the FSTL.

However, in [4], performance was given only for the case of a single-pole RC filter, and NRZ signaling format. In this report, the case for Manchester signaling format is given as well as for NRZ signals. Butterworth filters of order 2 and 3, and ideal low pass filters are also studied. In [4], the analysis method used for numerical computation was pretty complicated and hard to be generalized. In this report, a simple way for numerical computation is introduced which applies for most physical low pass filters.

Squaring loss is used as a parameter for performance analysis. Along with the design curves given, clock jitter and average slip rate can be determined. Comparison of the CSSL with the popular bit synchronizer, the Digital Data Transition Tracking Loop (DTTL) is also illustrated.

2. SYSTEM MODEL OF CSSL

The system model of the Cross-Spectrum Symbol Synchronizer Loop (CSSL) is given in Fig. 1. The baseband input signal $\sqrt{S_m(t)}$ is a PCM

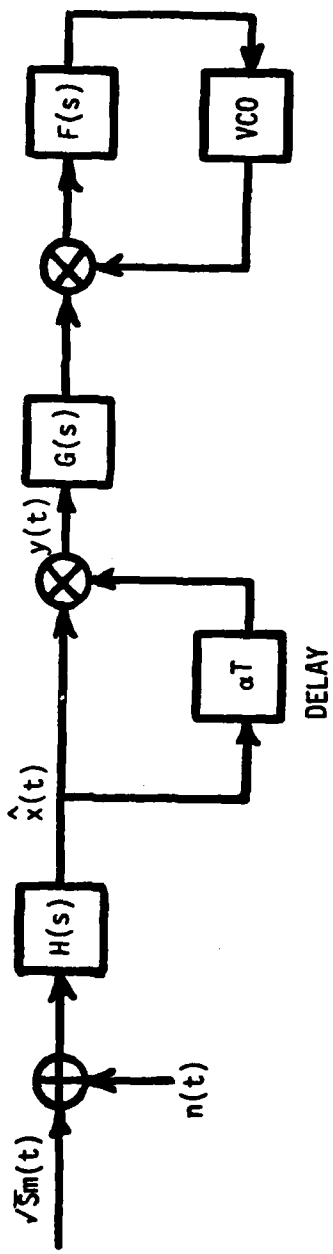


Figure 1. Cross-Spectrum Symbol Synchronizer.

signal. The additive noise is white Gaussian with two-sided spectral density $N_0/2$ watt/Hz. The power of the signal is S , and $m(t)$ is modeled as

$$m(t) = \sum_{i=-\infty}^{\infty} a_i p(t-iT) \quad (1)$$

where $a_i = \pm 1$ is the i -th data bit. The data is assumed to be binary and independent. The pulse waveshape $p(t)$ is assumed to have NRZ or Manchester (biphase) signaling format. Let the a priori probability of the data $a_i = 1$ be p , i.e. $P[a_i=1] = p$. Then, $P[a_i=-1] = q = 1-p$. The transition density p_t can be shown to be $p_t = 2pq$. For equal a priori probability $p = q$, $p_t = 50\%$.

The filter $H(s)$ plays an important role in determining the performance of the synchronizer. The shape of the transfer function and its 3 dB bandwidth are two important factors to be determined. Although a matched filter matched to the input signal pulse waveshape and transition density can be found theoretically, they are very difficult to be implemented. In practice, simple linear Butterworth filters are used. In this report, Butterworth filters of order $n = 1, 2, 3$ and ∞ (ideal low pass filter) are used for $H(s)$.

The filter $G(s)$ is a bandpass filter to pass the desired n -th harmonic frequency ($\omega_n = 2n\pi/T$) of the signal $y(t)$. Other harmonics are filtered out. This signal $z(t)$ is then fed into the phase-locked loop (PLL) for tracking.

3. PERFORMANCE ANALYSIS OF CSSL

The input to the filter $H(s)$ is

$$\begin{aligned}
 x(t) &= \sqrt{S} m(t) + n(t) \\
 &= \sqrt{S} \sum_{i=-\infty}^{\infty} a_i p(t-iT) + n(t)
 \end{aligned} \tag{2}$$

By using the Heaviside notation, the output signal $\hat{x}(t)$ is

$$\begin{aligned}
 \hat{x}(t) &= H(p)x(t) \\
 &= \sqrt{S} \hat{m}(t) + \hat{n}(t)
 \end{aligned} \tag{3}$$

where $\hat{m}(t) = H(p)m(t)$ is the output of the signal component, and the $\hat{n}(t) = H(p)n(t)$ is the output of the noise component. The signal $y(t)$ output of the delay and multiply circuit is

$$\begin{aligned}
 y(t) &= \hat{x}(t)\hat{x}(t-\alpha T) \\
 &= y_{ss}(t) + N_{sn}(t) + N_{nn}(t)
 \end{aligned} \tag{4}$$

where

$$\begin{aligned}
 y_{ss}(t) &= S\hat{m}(t)\hat{m}(t-\alpha T) \\
 N_{sn}(t) &= \sqrt{S}[\hat{m}(t)\hat{n}(t-\alpha T) + \hat{n}(t)\hat{m}(t-\alpha T)] \\
 N_{nn}(t) &= \hat{n}(t)\hat{n}(t-\alpha T)
 \end{aligned}$$

The $y_{ss}(t)$ is the signal x signal component, $N_{sn}(t)$ is the signal x noise component, and the $N_{nn}(t)$ is the noise x noise component of $y(t)$. Define an equivalent noise process

$$N(t) = N_{sn}(t) + N_{nn}(t) \tag{5}$$

We have

$$y(t) = y_{ss}(t) + N(t) \tag{6}$$

The $y_{ss}(t)$ process can be decomposed into two components,

$$y_{SS}(t) = \overline{y_{SS}(t)} + N_{SS}(t) \quad (7)$$

where

$$N_{SS}(t) = y_{SS}(t) - \overline{y_{SS}(t)} \quad (8)$$

and the overbar denotes statistical average. We assume the fluctuation of $y_{SS}(t)$ due to the data pattern (self-noise) is small [3,4], so that $y_{SS}(t)$ can be replaced by $\overline{y_{SS}(t)}$.

$\overline{y_{SS}(t)}$ can be written as

$$\overline{y_{SS}(t)} = SC(t) \quad (9)$$

with¹

$$C(t) = \sum_k \hat{p}(t-kT) \hat{p}(t-\alpha T-kT) + \sum_{\substack{k, n \\ n \neq k}} (p-q)^2 \hat{p}(t-nT) \hat{p}(t-\alpha T-kT) \quad (10)$$

Since $C(t)$ is periodic in t with period T , it can be expanded in a Fourier Series

$$C(t) = \sum_{n=-\infty}^{\infty} C_n e^{j\omega_n t} \quad (11)$$

where

$$\omega_n = \frac{2n\pi}{T}$$

and

$$C_n = \frac{1}{T} \int_0^T C(t) e^{-j\omega_n t} dt$$

¹In Eq. (10), we have adopted the lower case p for both pulse waveshape and the a priori probability $P[a_k=1] = p$, but there will be no confusion in the context.

After some algebra (see Appendix A), C_n can be expressed as

$$C_n = \frac{2pq}{\pi T} \int_{-\infty}^{\infty} \hat{P}(\omega) \hat{P}(\omega_n - \omega) e^{-j\omega \alpha T} d\omega \\ + \frac{(p-q)^2}{T^2} \sum_{k=-\infty}^{\infty} \hat{P}(\omega_n - \frac{2\pi k}{T}) \hat{P}(\frac{2\pi k}{T}) e^{-j(\omega_n - \frac{2\pi k}{T})\alpha T} \quad (12)$$

where $\hat{P}(\omega)$ is the Fourier Transform of the output pulse shape $\hat{p}(t)$.

Next, we need to evaluate the power spectrum of the equivalent noise $N(t)$. From (4), (5) we have

$$N(t) = \sqrt{S}[\hat{m}(t)\hat{n}(t-\alpha T) + \hat{m}(t-\alpha T)\hat{n}(t)] + \hat{n}(t)\hat{n}(t-\alpha T) \quad (13)$$

The autocorrelation of $N(t)$ is

$$R_N(\tau) = \overline{\langle N(t)N(t+\tau) \rangle} \\ = S[2R_{\hat{m}}^{\wedge}(\tau)R_{\hat{n}}^{\wedge}(\tau) + R_{\hat{m}}^{\wedge}(\tau-\alpha T)R_{\hat{n}}^{\wedge}(\tau+\alpha T) \\ + R_{\hat{m}}^{\wedge}(\tau+\alpha T)R_{\hat{n}}^{\wedge}(\tau-\alpha T)] + R_{\hat{n}\hat{n}}^{\wedge}(\tau) \quad (14)$$

where²

$$R_{\hat{m}}^{\wedge}(\tau) = \overline{\langle \hat{m}(t)\hat{m}(t+\tau) \rangle} \quad (15)$$

$$R_{\hat{n}}^{\wedge}(\tau) = \overline{\langle \hat{n}(t)\hat{n}(t+\tau) \rangle} \quad (16)$$

$$R_{\hat{n}\hat{n}}^{\wedge}(\tau) = R_{\hat{n}}^2(\alpha T) + R_{\hat{n}}^2(\tau) + R_{\hat{n}}(\tau-\alpha T)R_{\hat{n}}(\tau+\alpha T) \quad (17)$$

²Since $m(t)$ is a cyclostationary process, we need to take the time average also in $R_{\hat{m}}(\tau)$.

The spectrum of $N(t)$, $S_N(\omega)$, is the Fourier Transform of $R_N(\tau)$.

$$\begin{aligned} S_N(\omega) &= \underline{F}[R_N(\tau)] \\ &= S_{Sn}(\omega) + S_{nn}(\omega) \end{aligned} \quad (18)$$

where

$$\begin{aligned} S_{Sn}(\omega) &= S \int_{-\infty}^{\infty} [2R_m^{\wedge}(\tau)R_n^{\wedge}(\tau) + R_m^{\wedge}(\tau - \alpha T)R_n^{\wedge}(\tau + \alpha T) \\ &\quad + R_m^{\wedge}(\tau + \alpha T)R_n^{\wedge}(\tau - \alpha T)] e^{-j\omega\tau} d\tau \end{aligned} \quad (19)$$

and

$$S_{nn}(\omega) = \int_{-\infty}^{\infty} [R_n^2(\alpha T) + R_n^2(\tau) + R_n(\tau - \alpha T)R_n(\tau + \alpha T)] e^{-j\omega\tau} d\tau \quad (20)$$

Let

$$S_m^{\wedge}(\omega) = \underline{F}[R_m^{\wedge}(t)] \quad (21)$$

and

$$S_n^{\wedge}(\omega) = \underline{F}[R_n^{\wedge}(\tau)]$$

$S_{Sn}(\omega)$ and $S_{nn}(\omega)$ can be written as

$$S_{Sn}(\omega) = \frac{S}{\pi} \int_{-\infty}^{\infty} S_m^{\wedge}(x) S_n^{\wedge}(\omega - x) \{1 + \cos[(\omega - 2x)\alpha T]\} dx \quad (22)$$

$$S_{nn}(\omega) = 2\pi R_n^2(\alpha T) \delta(\omega) + \frac{1}{2\pi} \int_{-\infty}^{\infty} S_n^{\wedge}(x) S_n^{\wedge}(\omega - x) [1 + e^{j(\omega - 2x)\alpha T}] dx \quad (23)$$

To evaluate $S_m^{\wedge}(\omega)$, we first find $S_m(\omega)$ (see Appendix B), and make use of the relation

$$S_m^{\wedge}(\omega) = |H(\omega)|^2 S_m(\omega) \quad (24)$$

which yields

$$S_m^{\wedge}(\omega) = \frac{1}{T} |P(\omega)|^2 |H(\omega)|^2 \left\{ 4pq + \frac{2\pi}{T} (p-q)^2 \sum_l \delta(\omega + \frac{2\pi l}{T}) \right\} \quad (25)$$

$$S_n^{\wedge}(\omega) = |H(\omega)|^2 S_n(\omega) = \frac{N_0}{2} |H(\omega)|^2 \quad (26)$$

Substituting (25) and (26) into (22) and (23) with $z = xT$, at

$\omega = \omega_n \neq 0$, we obtain

$$\begin{aligned} S_{sn}(\omega_n) &= SN_0 \left\{ \frac{2pq}{\pi} \int_{-\infty}^{\infty} [1 + \cos[2\alpha(n\pi - z)]] |H(\frac{2n\pi - z}{T})|^2 \frac{1}{T^2} |P(\frac{z}{T})|^2 |H(\frac{z}{T})|^2 dz \right. \\ &+ (p-q)^2 \sum_{l=-\infty}^{\infty} [1 + \cos[2\pi\alpha(n+2l)]] |H(\frac{2\pi}{T}(n+2l))|^2 \frac{1}{T^2} |P(\frac{2\pi l}{T})|^2 |H(\frac{2\pi l}{T})|^2 \left. \right\} \quad (27) \end{aligned}$$

$$S_{nn}(\omega_n) = \frac{N_0^2}{8\pi T} \int_{-\infty}^{\infty} |H(\frac{z}{T})|^2 |H(\frac{2n\pi - z}{T})|^2 [1 + e^{j2\alpha(n\pi - z)}] dz \quad (28)$$

As mentioned above, the input to the PLL is a single tone (ω_n) plus narrowband equivalent noise. By using the linear PLL theory [5], the mean-square phase tracking jitter is given by

$$\begin{aligned} \sigma_{\phi_n}^2 &= \frac{[S_{sn}(\omega_n) + S_{nn}(\omega_n)] W_L}{S^2 [|C_n|^2 + |C_{-n}|^2]} \\ &= \frac{[S_{sn}(\omega_n) + S_{nn}(\omega_n)] B_L}{S^2 |C_n|^2} \quad (29) \end{aligned}$$

where W_L is the two-sided loop bandwidth $W_L = 2B_L$, and B_L is the single-sided bandwidth. The mean-square phase tracking jitter can be expressed in terms of the "squaring loss" S_L

$$\sigma_{\phi_n}^2 \triangleq \frac{1}{\rho S_L} \quad (30)$$

where

$$\rho \triangleq \frac{S}{\left(\frac{N_0}{2}\right)W_L} = \frac{2R_s}{W_L T} \quad (31)$$

$$R_s = \frac{ST}{N_0} \quad (32)$$

Then the squaring loss S_L is expressed as

$$S_L = \frac{SN_0 |C_n|^2}{S_{sn}(\omega_n) + S_{nn}(\omega_n)} < 1 \quad (33)$$

The relative timing error, normalized to a symbol period, is defined as

$$\lambda_n \triangleq \frac{\phi_n}{2n\pi} \quad (34)$$

The variance of this error is

$$\sigma_{\lambda_n}^2 = \frac{\sigma_{\phi_n}^2}{(2n\pi)^2} = \frac{1}{(2n\pi)^2} \cdot \frac{1}{\rho S_L} \quad (35)$$

The "clock jitter" is defined as σ_{λ_n} which is an important parameter for synchronizer performance.

Another important parameter in tracking performance analysis is the average cycle slipping rate \bar{S} . From [5, Ch. 9]

$$\bar{S} = \frac{W_L}{\alpha_s} \frac{\cosh \pi \beta}{\pi^2 |I_{j\beta}(\alpha_s)|^2} \quad (36)$$

For $\beta = 0$, $\alpha_s = \rho S_L$ the normalized slip rate \bar{S}/W_L is

$$\frac{\bar{S}}{W_L} = \frac{1}{\rho S_L \pi^2 |I_0(\rho S_L)|^2} \quad (37)$$

where $I_0(x)$ is the modified Bessel function of the first kind of order zero.

The filter used in $H(s)$ is a n -th order Butterworth filter characterized by

$$|H(\omega)|^2 = \frac{1}{1 + (\frac{\omega}{B})^{2n}} \quad (38)$$

where $f_0 = B/2\pi$ is the 3 dB cutoff frequency. The transfer function of the Butterworth filter is given by

$$H(j\omega) = \frac{(BT)^n}{\prod_{i=1}^n (j\omega T - BT S_i)} \quad i = 1, 2, \dots, n \quad (39)$$

with

$$S_i = \exp[j\pi(\frac{1}{2} + (2i-1)/2n)]$$

When $n=1$, the Butterworth filter is a single pole RC filter. When $n \rightarrow \infty$, it approximates an ideal low pass filter.

The signaling format for the input signal is NRZ and Bi- ϕ . Their Fourier Transform of the pulse shapes are given by

$$\text{NRZ: } P(\omega) = \frac{1}{j\omega} [1 - e^{-j\omega T}] \quad (40)$$

$$\text{Bi-}\phi: P(\omega) = \frac{1}{j\omega} [1 - 2e^{-j\omega T/2} + e^{-j\omega T}] \quad (41)$$

Substituting (40) and (41) in (12), we obtain

NRZ:

$$C_n = \begin{aligned} & (p-q)^2 H^2(0) + \frac{2pq}{\pi} \int_{-\infty}^{\infty} H\left(\frac{z}{T}\right) H\left(\frac{-z}{T}\right) \text{sinc}^2\left(\frac{z}{2}\right) e^{-j\alpha z} dz; \quad n=0 \\ & \frac{(-1)^n 2pq}{\pi} \int_{-\infty}^{\infty} H\left(\frac{z}{T}\right) H\left(\frac{2n\pi - z}{T}\right) \text{sinc}\left(\frac{z}{2}\right) \text{sinc}\left(\frac{2n\pi - z}{2}\right) e^{-j\alpha z} dz; \quad n \neq 0 \end{aligned} \quad (42)$$

Bi- ϕ :

$$C_n = \begin{aligned} & \frac{(-1)^n 2pq}{\pi} \int_{-\infty}^{\infty} H\left(\frac{z}{T}\right) H\left(\frac{2n\pi - z}{T}\right) \left(\frac{z}{4}\right) \left(\frac{z - 2n\pi}{4}\right) \text{sinc}^2\left(\frac{z}{4}\right) \text{sinc}^2\left(\frac{z - 2n\pi}{4}\right) e^{-j\alpha z} dz \\ & + (-1)^n (p-q)^2 \sum_{k=\pm 1, 3, \dots} H\left(\frac{2\pi k}{T}\right) H\left(\frac{2n\pi - 2k\pi}{T}\right) \left(\frac{\pi k}{2}\right) \text{sinc}^2\left(\frac{\pi k}{2}\right) \left[\frac{(k-n)\pi}{2}\right] \\ & \quad \cdot \text{sinc}^2\left[\frac{(k-n)\pi}{2}\right] e^{-j(n-k)2\pi\alpha} \end{aligned} \quad (43)$$

For Bi- ϕ , when n is even (which is the case for tracking), C_n is further simplified to

$$C_n = \begin{aligned} & \frac{2pq}{\pi} \int_{-\infty}^{\infty} H\left(\frac{z}{T}\right) H\left(\frac{2n\pi - z}{T}\right) \frac{z(z - 2n\pi)}{16} \text{sinc}^2\left(\frac{z}{4}\right) \text{sinc}^2\left(\frac{z - 2n\pi}{4}\right) e^{-j\alpha z} dz \\ & + \frac{4(p-q)^2}{\pi^2} \sum_{k \text{ odd}} H\left(\frac{2\pi k}{T}\right) H\left(\frac{2\pi(n-k)}{T}\right) \frac{e^{-j2\pi(n-k)\alpha}}{k(k-n)} \end{aligned} \quad (44)$$

4. NUMERICAL RESULTS

In this section, numerical results for the CSSL performance on NRZ and Bi- ϕ signaling formats are provided. Here Equations (27), (28), (42), and (43) are evaluated directly by numerical methods, rather than first expanded in series as done in [4]. In this way, different transfer functions $H(\omega)$ of filters can be easily substituted numerically, whereas the method of series expansion will involve a lot of calculation.

Fig. 2 plots the normalized harmonic power for the case of Bi- ϕ , $\alpha = 0.5$, $p = 0.5$, and single pole RC filter. Fig. 3 plots the same case except for $\alpha = 0.22$. For the case of interest, $f_0T = 3.0$, the second harmonic ($n=2$) component, and delay $\alpha = 0.22$ should be chosen since it has a larger harmonic power input to the PLL for tracking. Later on it will be shown this case indeed yields a larger squaring loss S_L (smaller clock jitter). Fig. 4 plots the harmonic power for NRZ. This figure suggests the first harmonic ($n=1$) should be chosen.

Fig. 5 plots the S_L in dB vs the filter time-bandwidth product f_0T for Bi- ϕ , RC filter, $R_s = 5$ dB, $n = 2$, and various values of α . It confirms for $F_0T = 3.0$, $\alpha = 0.22$ is the optimum value. As compared to Fig. 6, which has the same conditions except for $n=1$, the case $\alpha = 0.22$, $n = 2$, provides the optimal condition for tracking. Fig. 7 plots the same case for NRZ format. In this case, $\alpha = 0.5$, $n = 1$ provides the optimal condition. For small values of f_0T (say $f_0T < 1.5$), the assumption that the pattern noise (e.g (8)) is negligible may not hold [6]. Therefore, the values of S_L is valid only for large f_0T .

Fig. 8 plots S_L vs f_0T for Bi- ϕ and different filters. It is shown that for Bi- ϕ , 2nd and 3rd order Butterworth filters have a similar

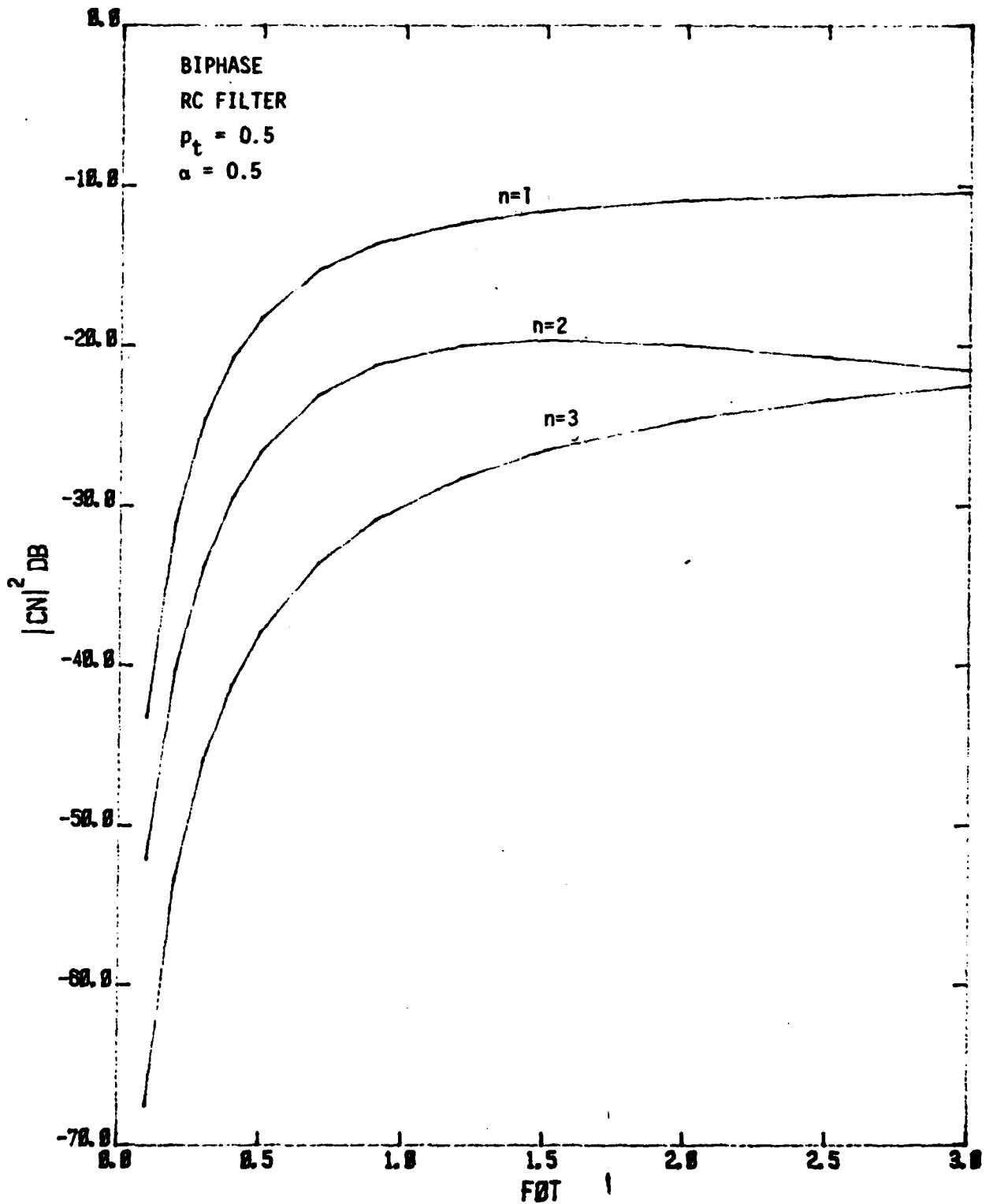


Figure 2. Normalized Harmonic Power Versus Filter Time Bandwidth Product.

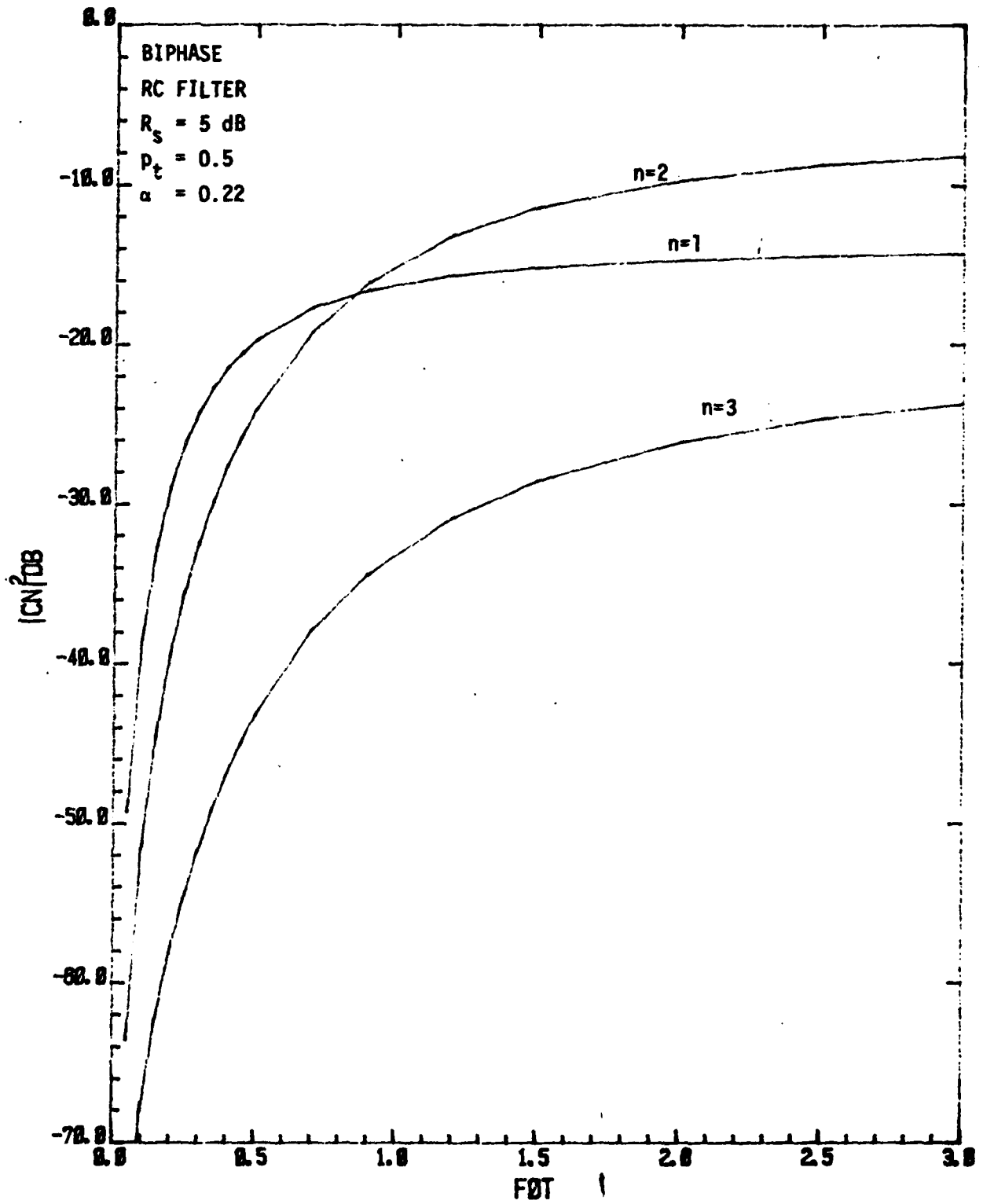


Figure 3. Normalized Harmonic Power vs. Filter Time Bandwidth Product.

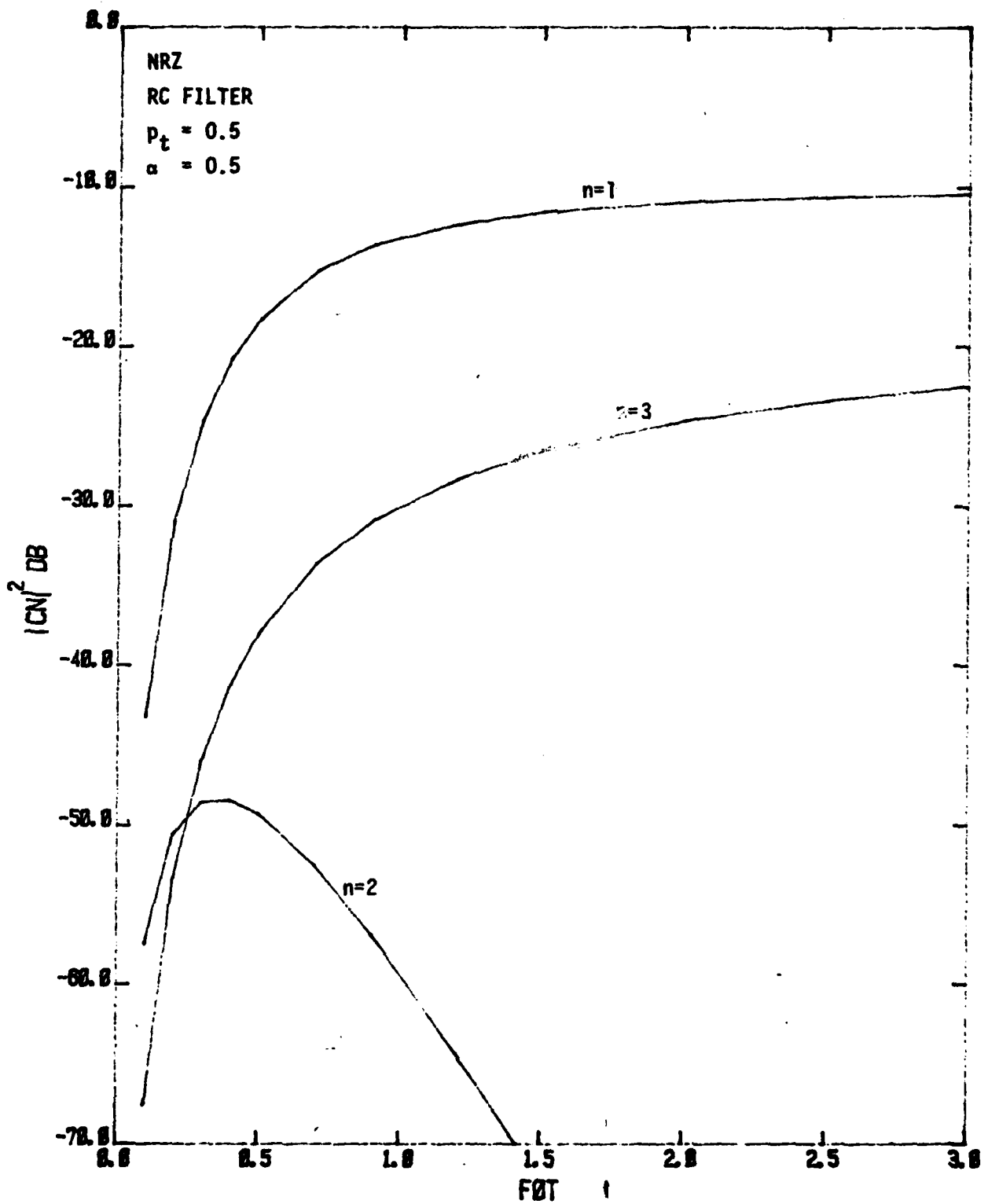


Figure 4. $|C_n|^2$ versus f_0T

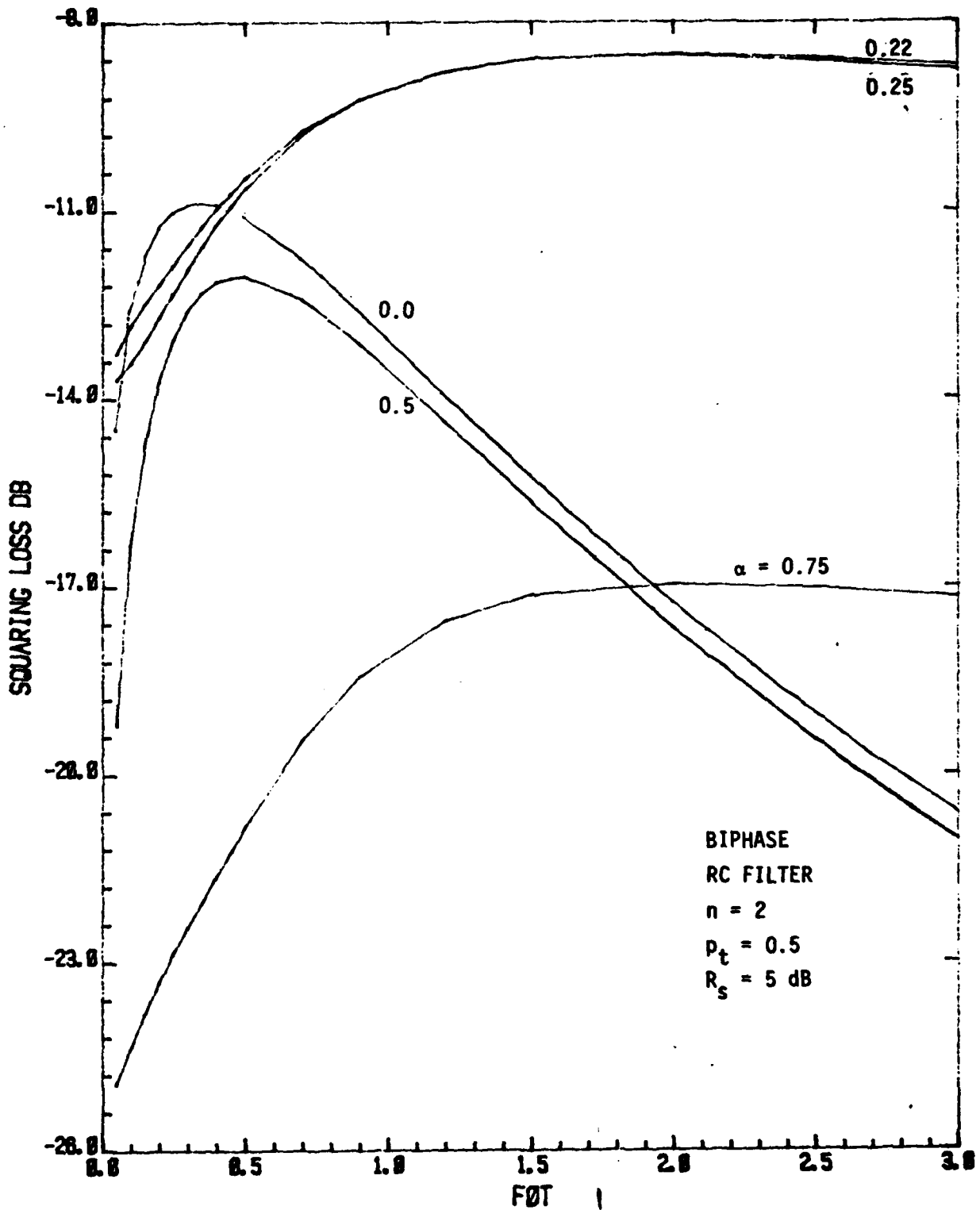


Figure 5. S_L vs f_0T for Various α , Biphase Format.

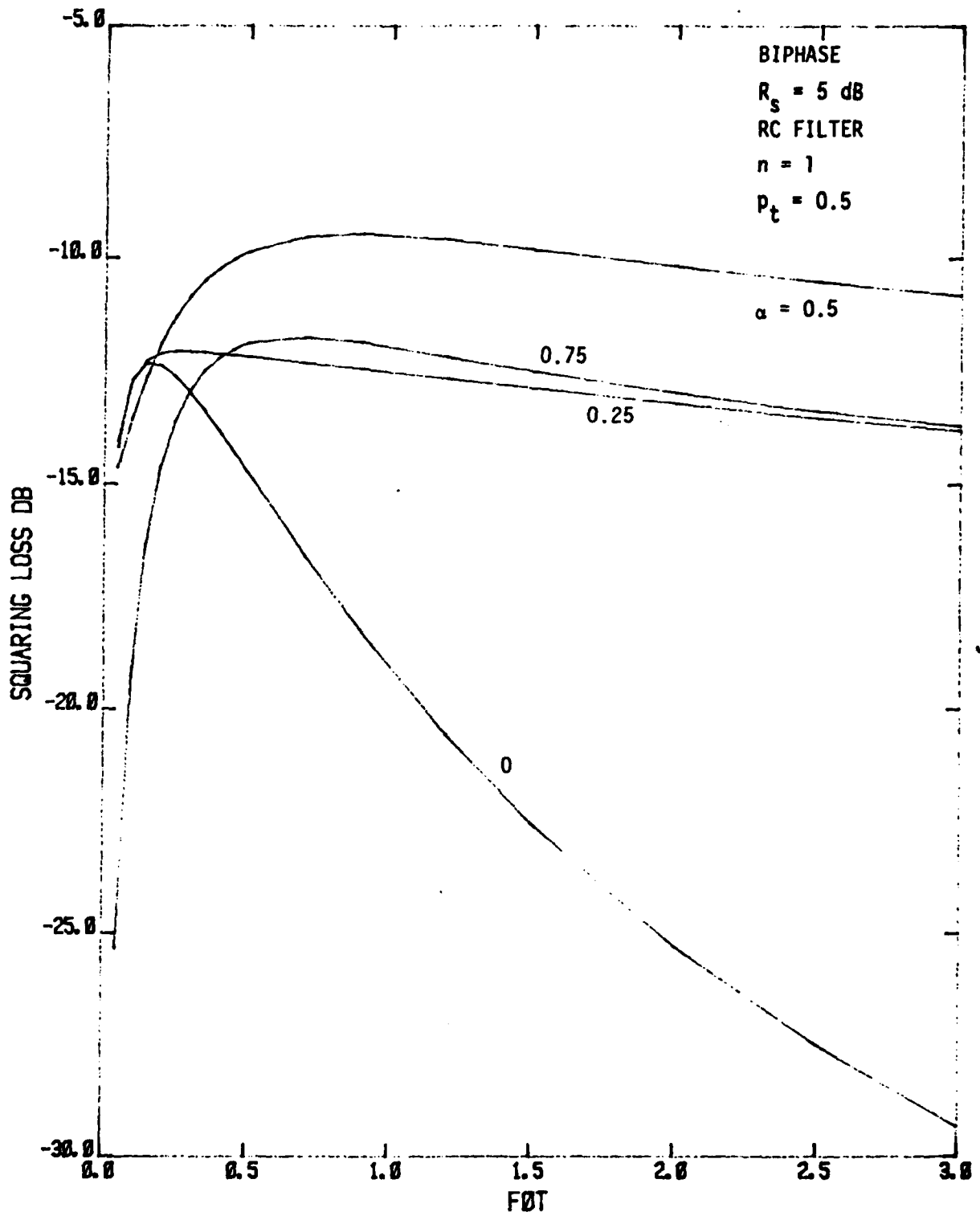


Figure 6. S_L vs f_0T for Various α , Biphase Format.

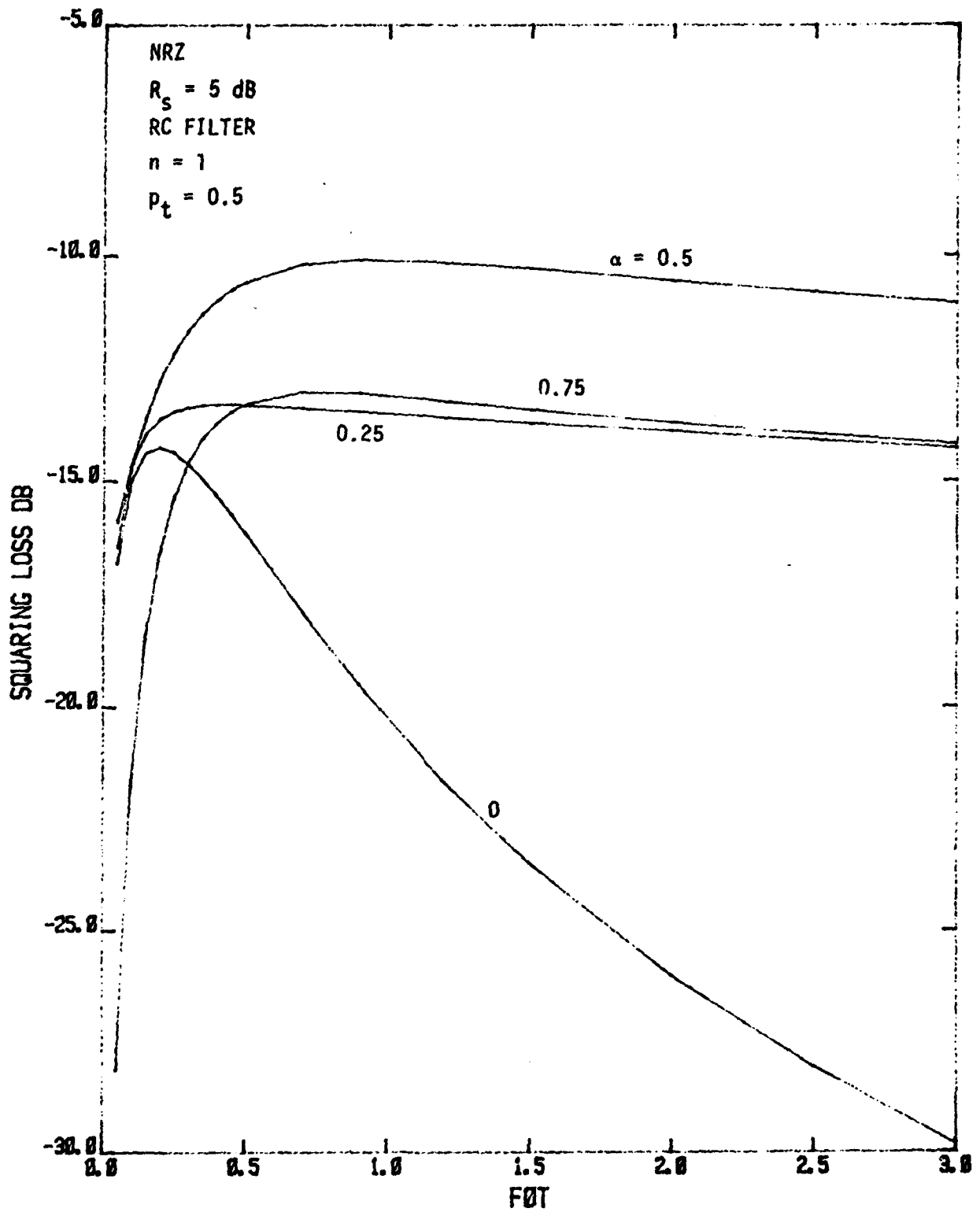


Figure 7. S_L vs $f_0 T$ for Various α , NRZ Format.

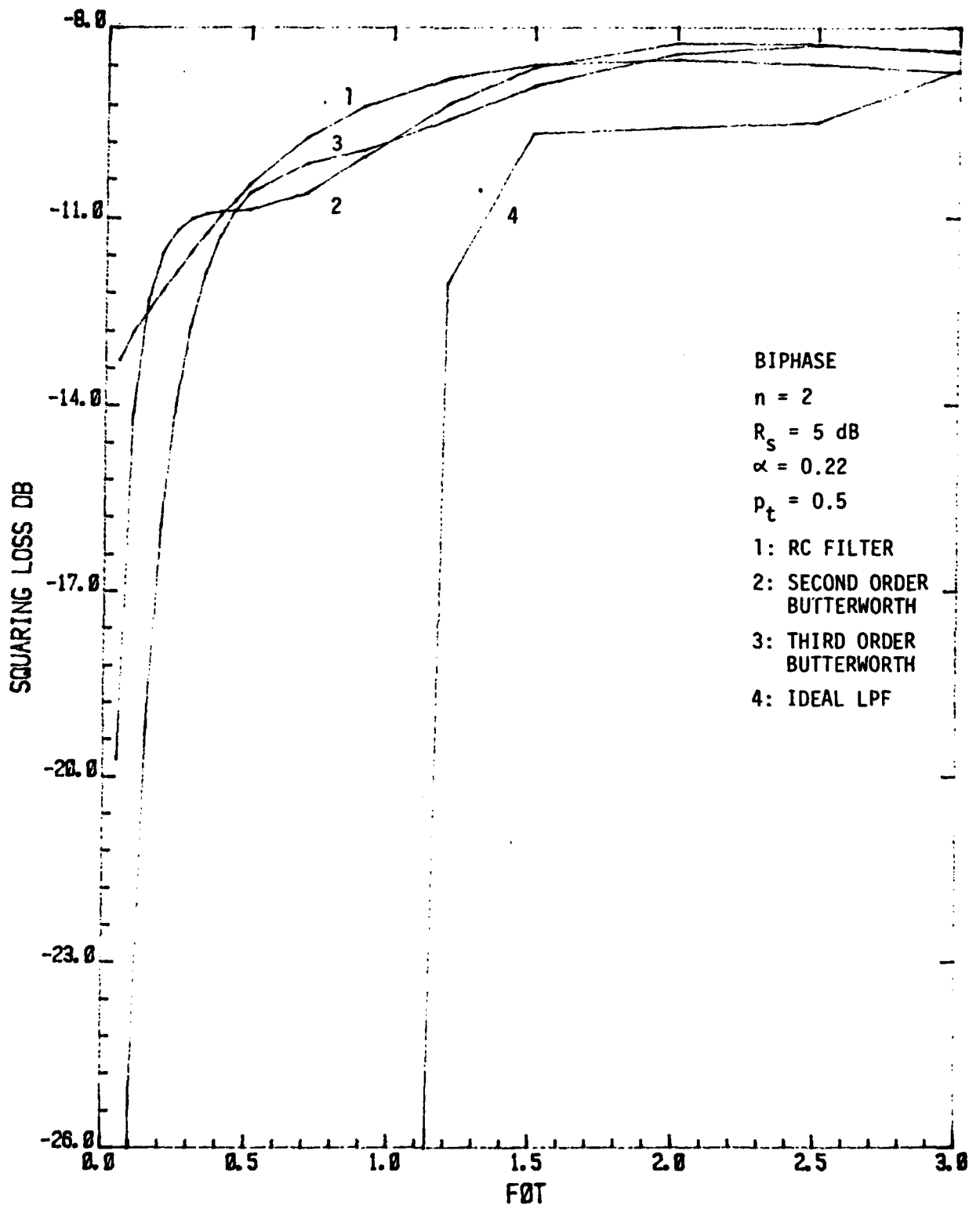


Figure 8. S_L vs f_0T for Biphase and Different Filters.

performance and are better than (for $f_0T = 3.0$) the RC filter and the ideal LPF. Fig. 9 plots the same case for NRZ format.

Figs. 10 and 11 plot S_L vs R_S for Bi- ϕ and NRZ, respectively. It shows that Bi- ϕ has a better performance than the NRZ in terms of S_L . For Bi- ϕ , the 2nd and 3rd order Butterworth filters have a very close performance.

Fig. 12 plots S_L vs the data transition density p_t for Bi- ϕ , $R_S = 5$ dB, 2nd order Butterworth filter, and various values of α . For the same α , S_L is larger for smaller p_t since for Bi- ϕ format, smaller p_t will arrive on the average a larger number of zero-crossings which in turn will yield a better performance in tracking. Figs. 13 and 14 plot the same case for $R_S = 15$ dB and -5 dB, respectively. For $R_S = -5$ dB, $\alpha = 0.25$ is the optimum value, whereas for larger R_S , $\alpha = 0.22$ is the optimum. Fig. 15 plots S_L vs p_t for the NRZ signaling format. As expected, S_L decreases when p_t decreases, since for NRZ the waveform will look like a DC signal when p_t is small, which is very difficult for tracking.

Figs. 16 and 17 are two design curves in terms of S_L . Fig. 16 plots the clock jitter σ_λ versus S_L for ρ ranging from 20 dB to 43 dB. If the S_L at a R_S value is known, the clock jitter can be found for the corresponding ρ . Recall that ρ is a function of R_S and W_{LT} . Fig. 17 plots the average normalized slip rate versus S_L for ρ ranging from 10 dB to 40 dB. Fig. 17 is used for sinusoidal signal tracking (e.g. CSSL). Given these two curves, the performance of the CSSL can be presented in terms of the S_L only.

5. PERFORMANCE COMPARISON BETWEEN CSSL AND DTTL

Performance comparison between CSSL and DTTL can be done in terms

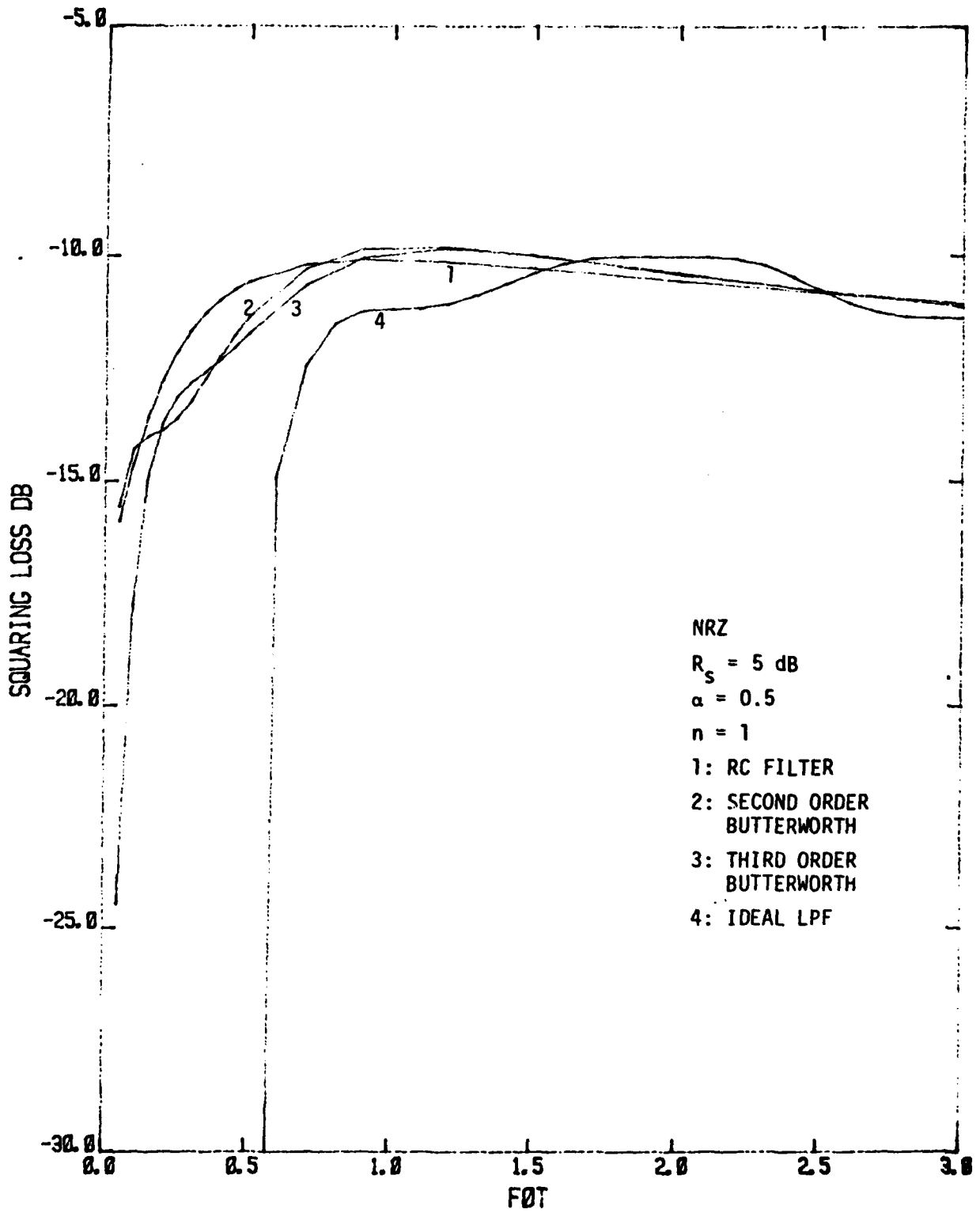


Figure 9. S_L Vs F_0T for NRZ and Different Filters.

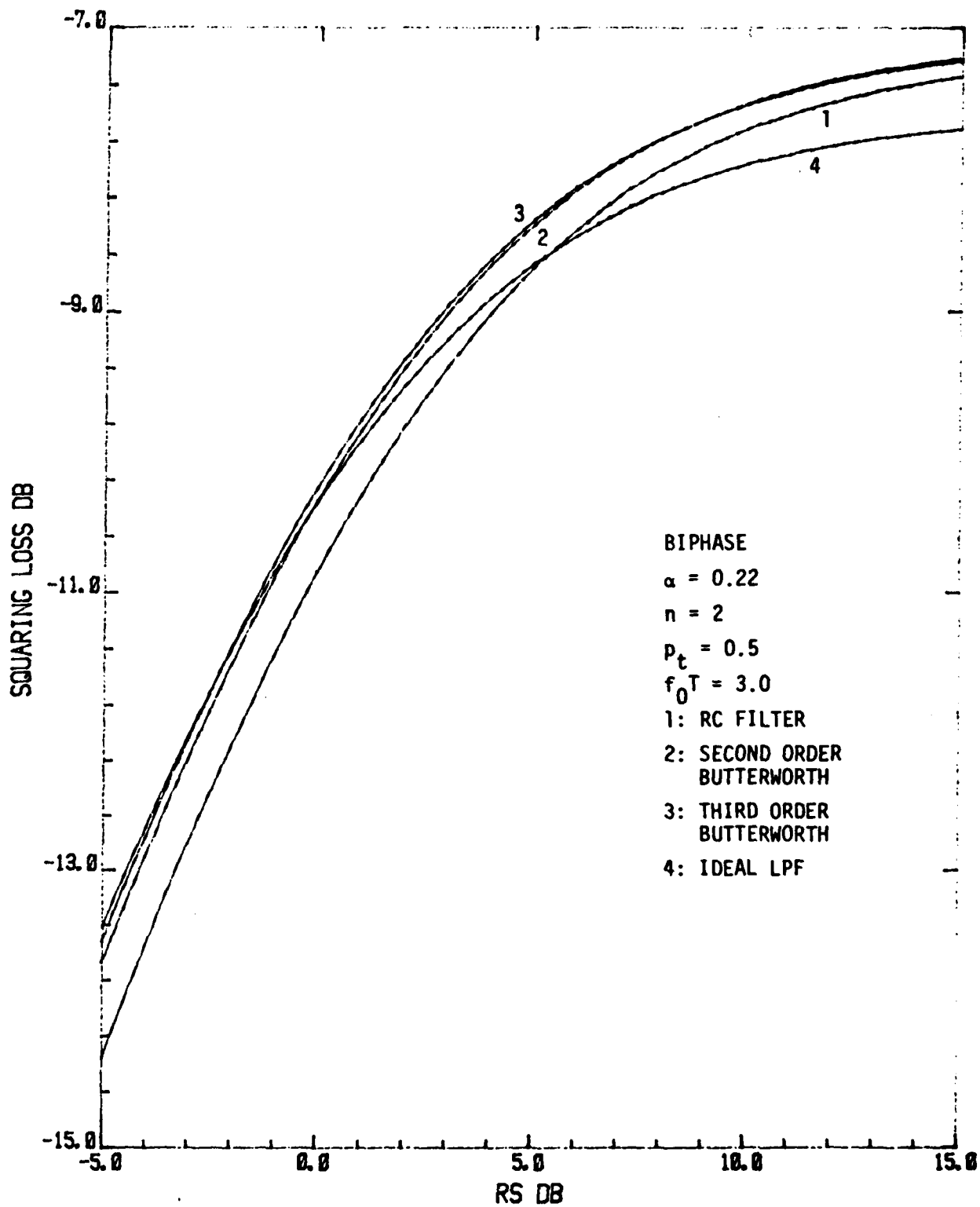


Figure 10. S_L vs R_S for Biphase and Different Filters.

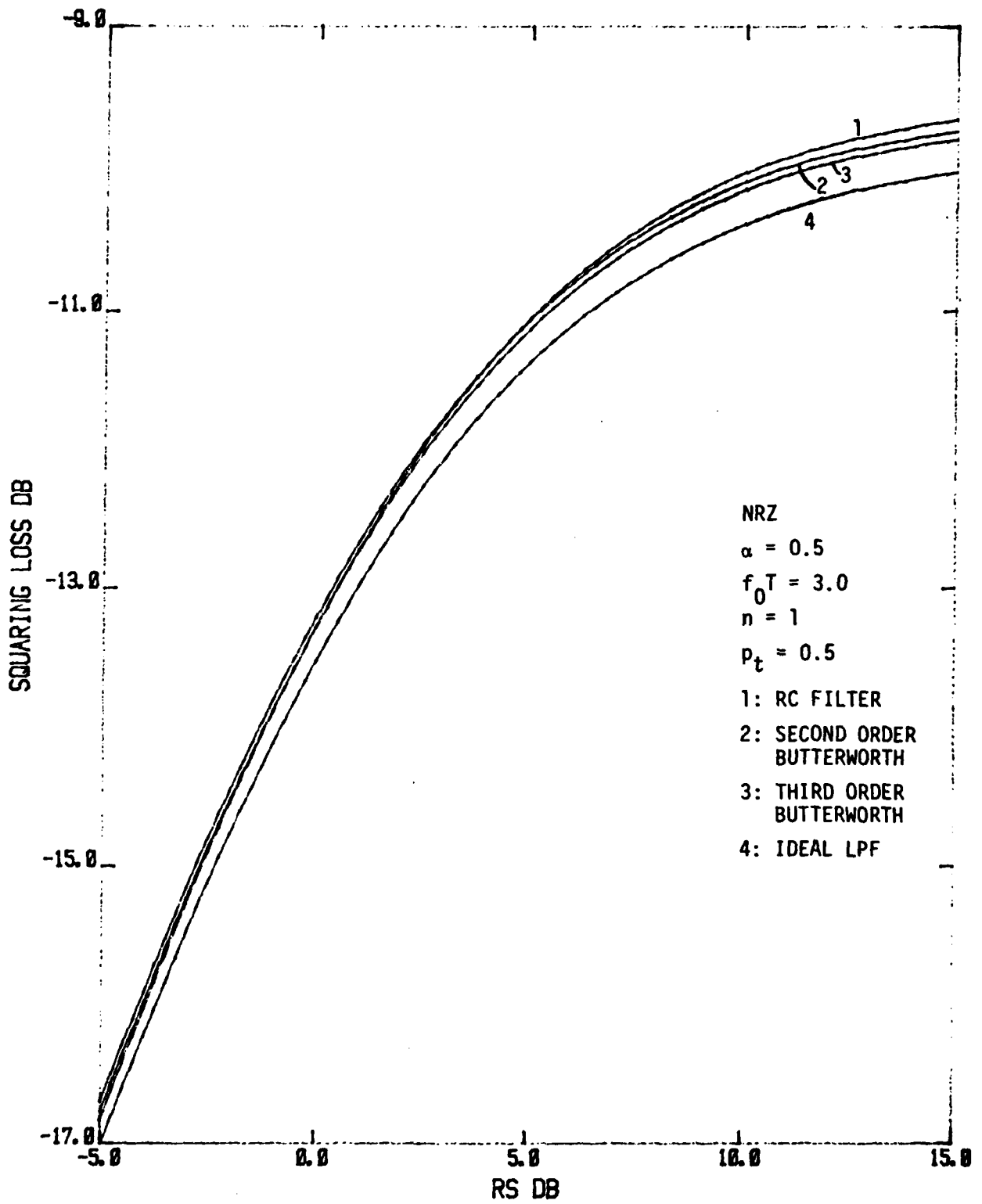


Figure 11. S_L vs R_s for NRZ and Different Filters.

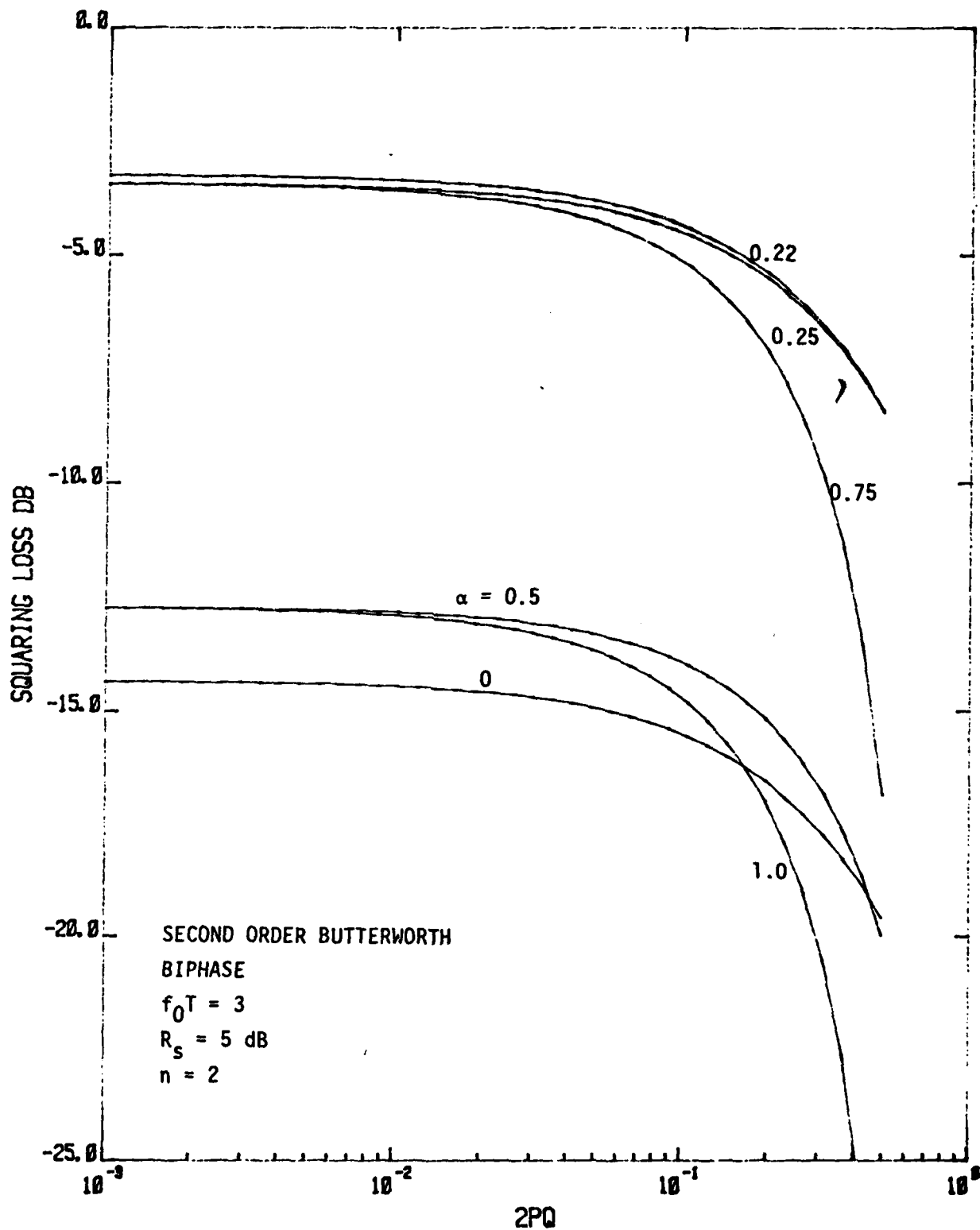


Figure 12. S_L vs p_t for Biphaser and Various α , $R_s = 5 \text{ dB}$.

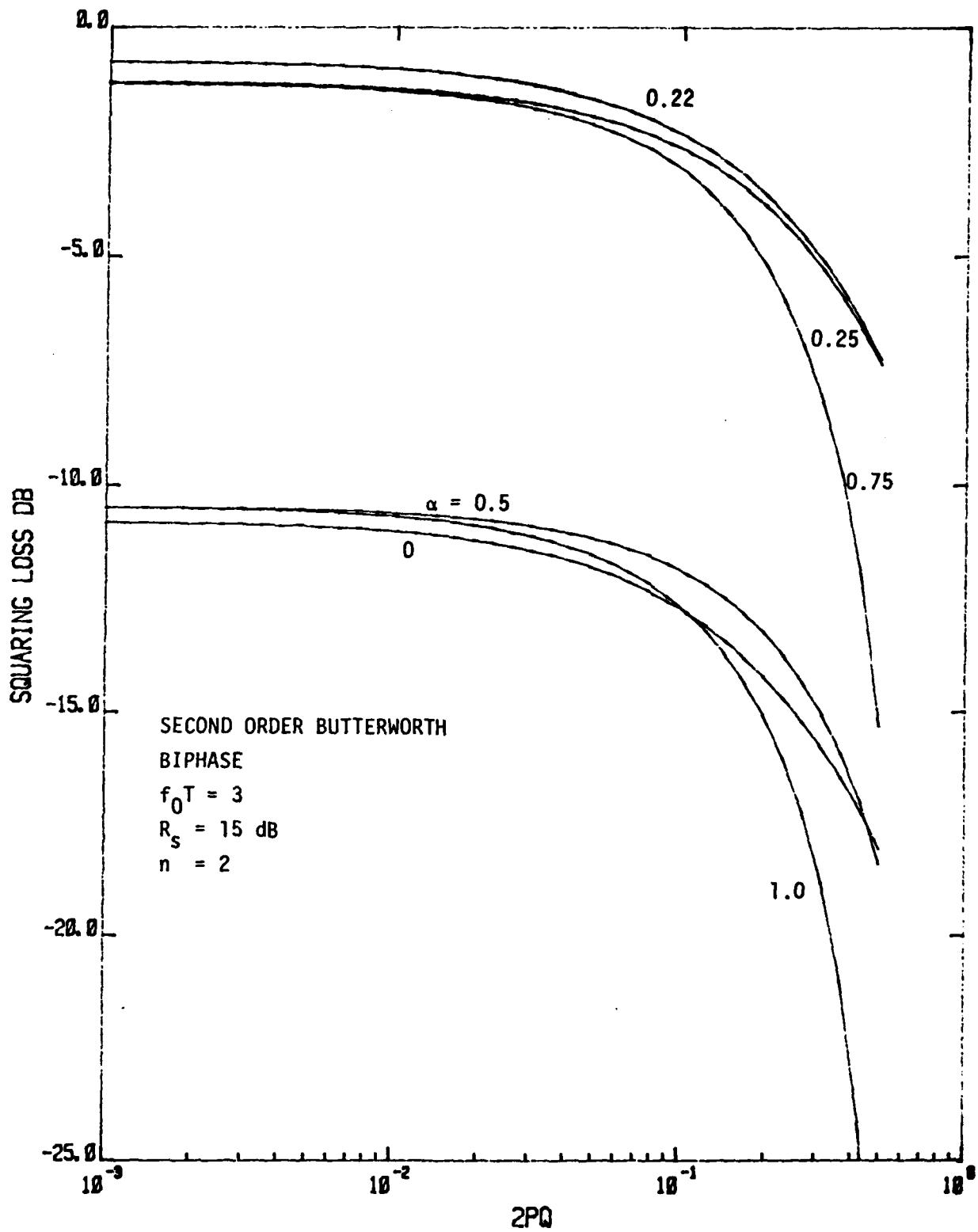


Figure 13. S_L vs p_t for Biphasic and Various α , $R_s = 15 \text{ dB}$.

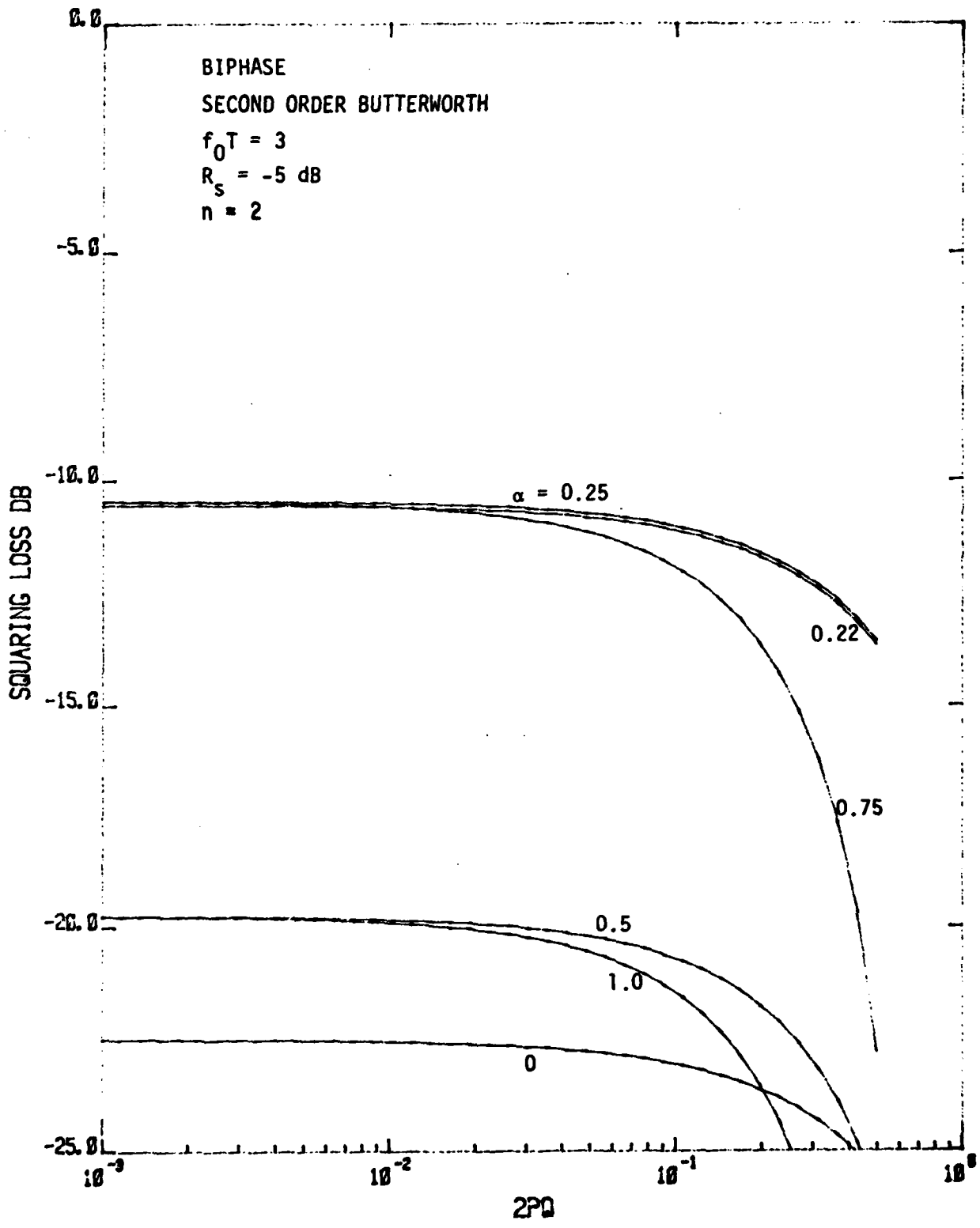


Figure 14. S_L vs p_t for Biphase and Various α , $R_s = -5 \text{ dB}$

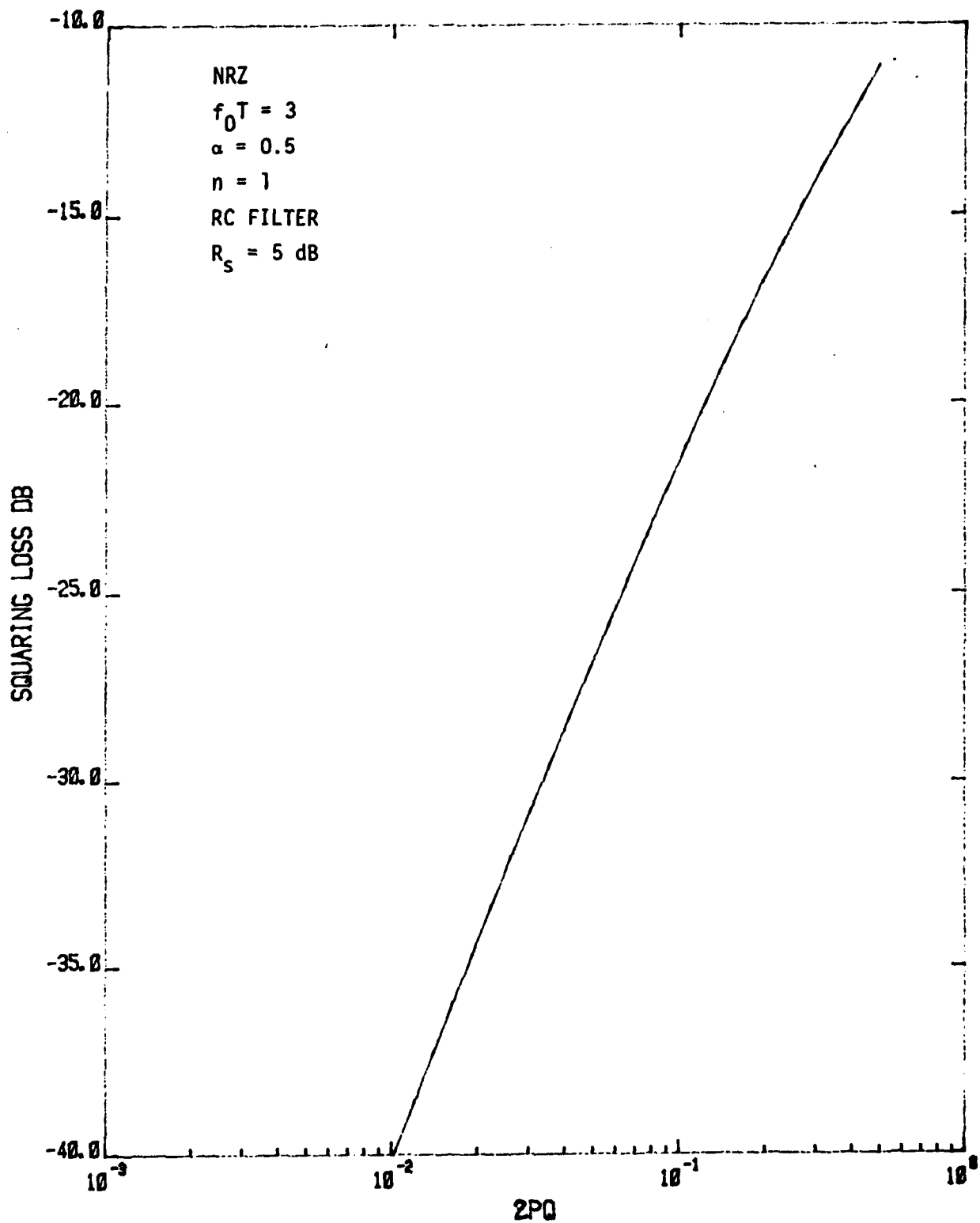


Figure 15. S_L vs p_t for NRZ and Various α .

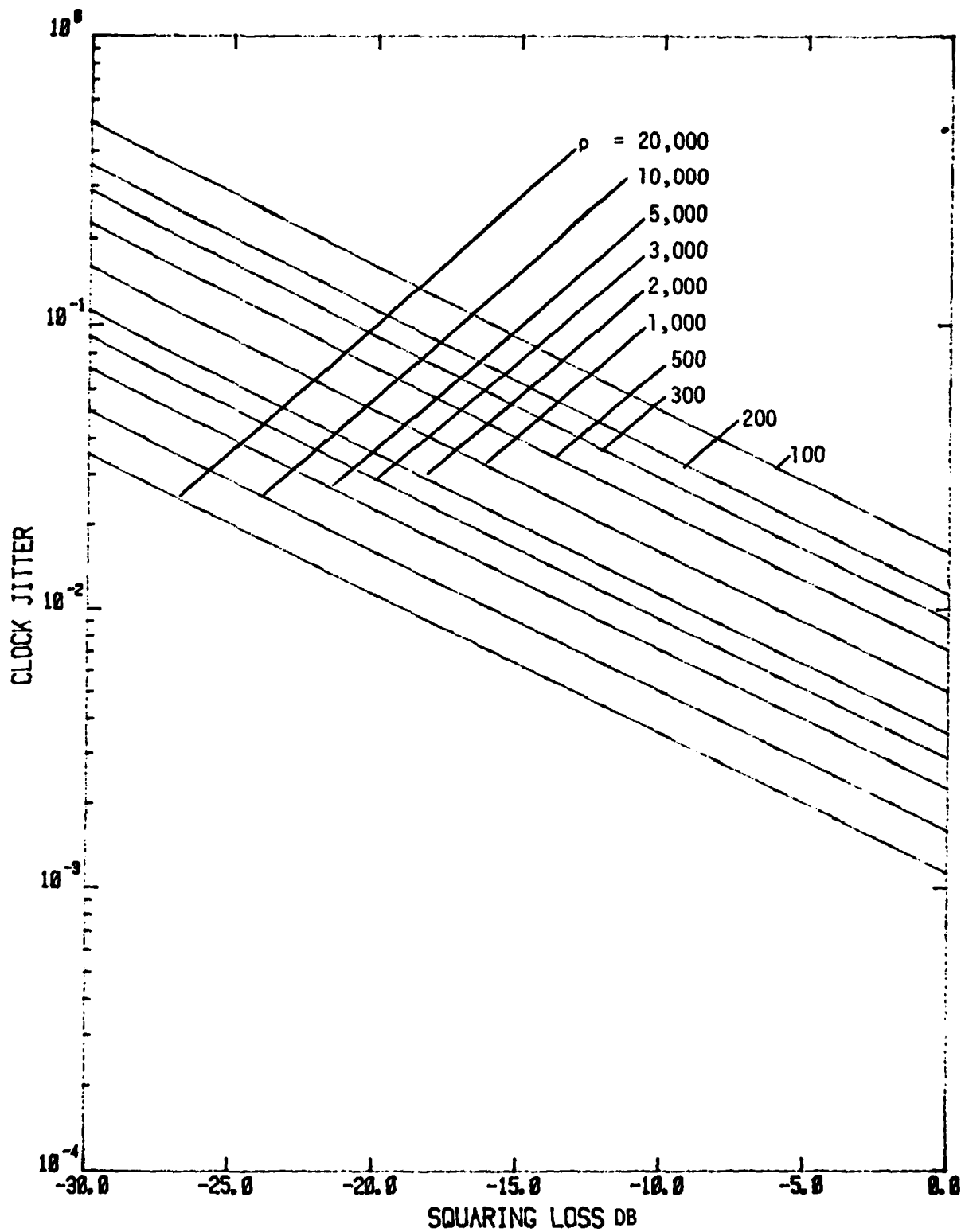


Figure 16. Clock Jitter vs S_L .

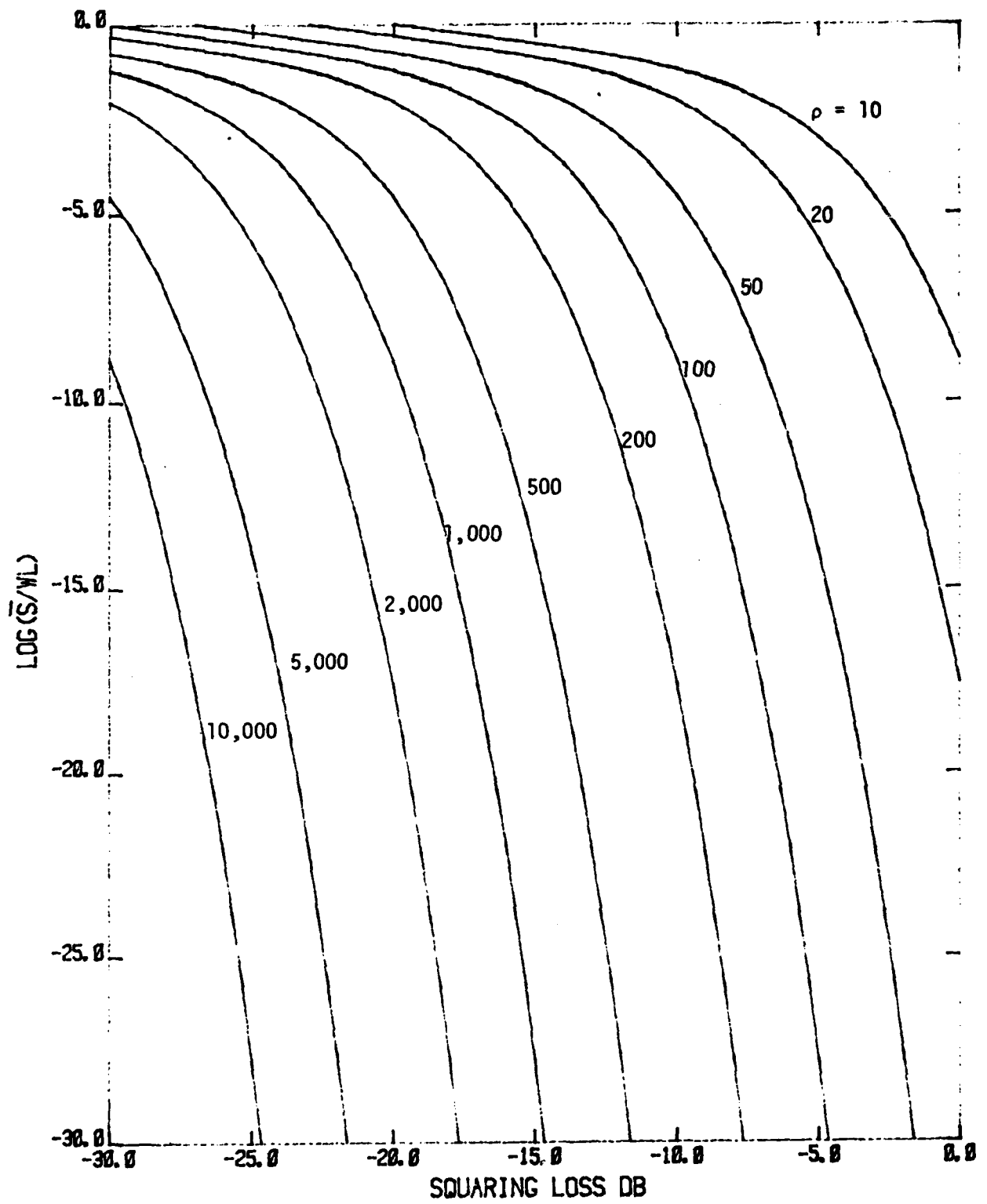


Figure 17. \bar{S}/W_L vs S_L for Sinusoidal PLL.

of S_L which is equivalently the clock jitter. Fig. 18 plots plots the S_L versus R_S for DTTL, NRZ signaling format, $p_t = 0.5$, with the window ξ_0 as a parameter. Fig. 19 plots the same case for bi-phase format. A brief derivation of the S_L for DTTL is given in Appendix C.

Comparing Figs. 10 and 19, for Bi- ϕ , the CSSL has a comparable performance with the DTTL with $\xi_0 = 0.5$. Comparing Figs. 11 and 18, the performance of the CSSL with NRZ format and RC filter is comparable with the DTTL with $\xi_0 = 0.45$ for $R_S = 15$ dB, and with $\xi_0 = 0.7$ for $R_S = -5$ dB.

This comparison may not be valid in the strict sense since the DTTL has assumed a wideband signal but the CSSL in this case has assumed $f_0T = 3.0$. The CSSL has an advantage of simpler hardware implementation (easier to maintain and more economical) comparing to the DTTL which may be an important consideration. Yet the DTTL could have still better performance by reducing the window width.

6. SUMMARY

The CSSL has the optimum performance when $\alpha = 0.5$, i.e. a half-symbol delay time, for NRZ signaling format. For Bi- ϕ signals, optimum performance is reached when $\alpha = 0.25$ for small R_S (say $R_S < 0$ dB), and $\alpha = 0.22$ for high R_S . The first harmonic should be the frequency to be tracked for NRZ while the second harmonic should be used for Bi- ϕ signals.

Tracking performance, clock jitter and average slip rate, are given in terms of the squaring loss. Since the average slip rate is very sensitive to the value of S_L (see Fig. 17), optimization of average slip rate (or S_L) over the filter time-bandwidth product f_0T seems possible (see Figs. 5 and 7). However, since the optimal f_0T value is pretty small (< 1) for NRZ, it is only of interest for very narrow-band

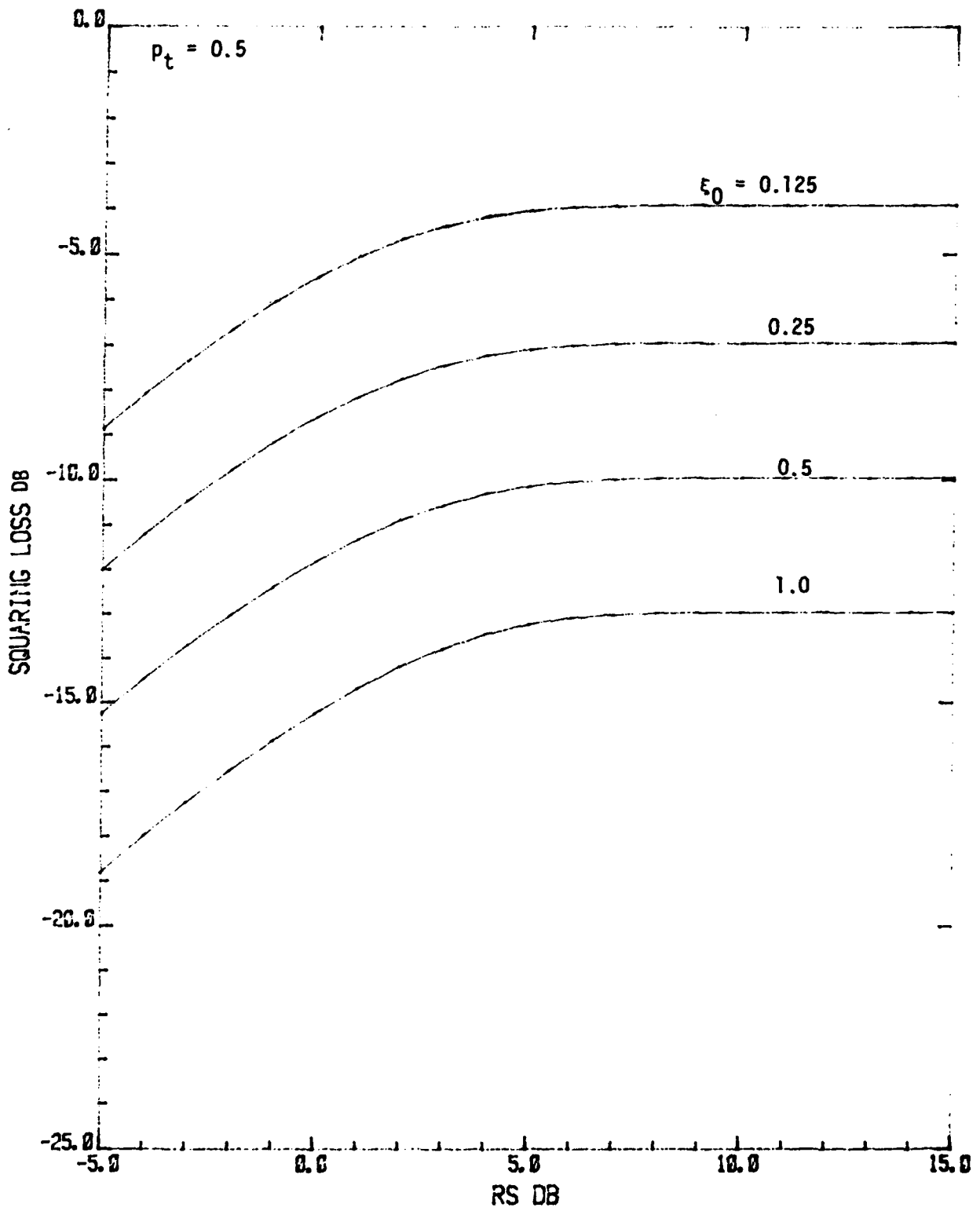


Figure 18. S_L vs R_s for DTTL, NRZ Format.

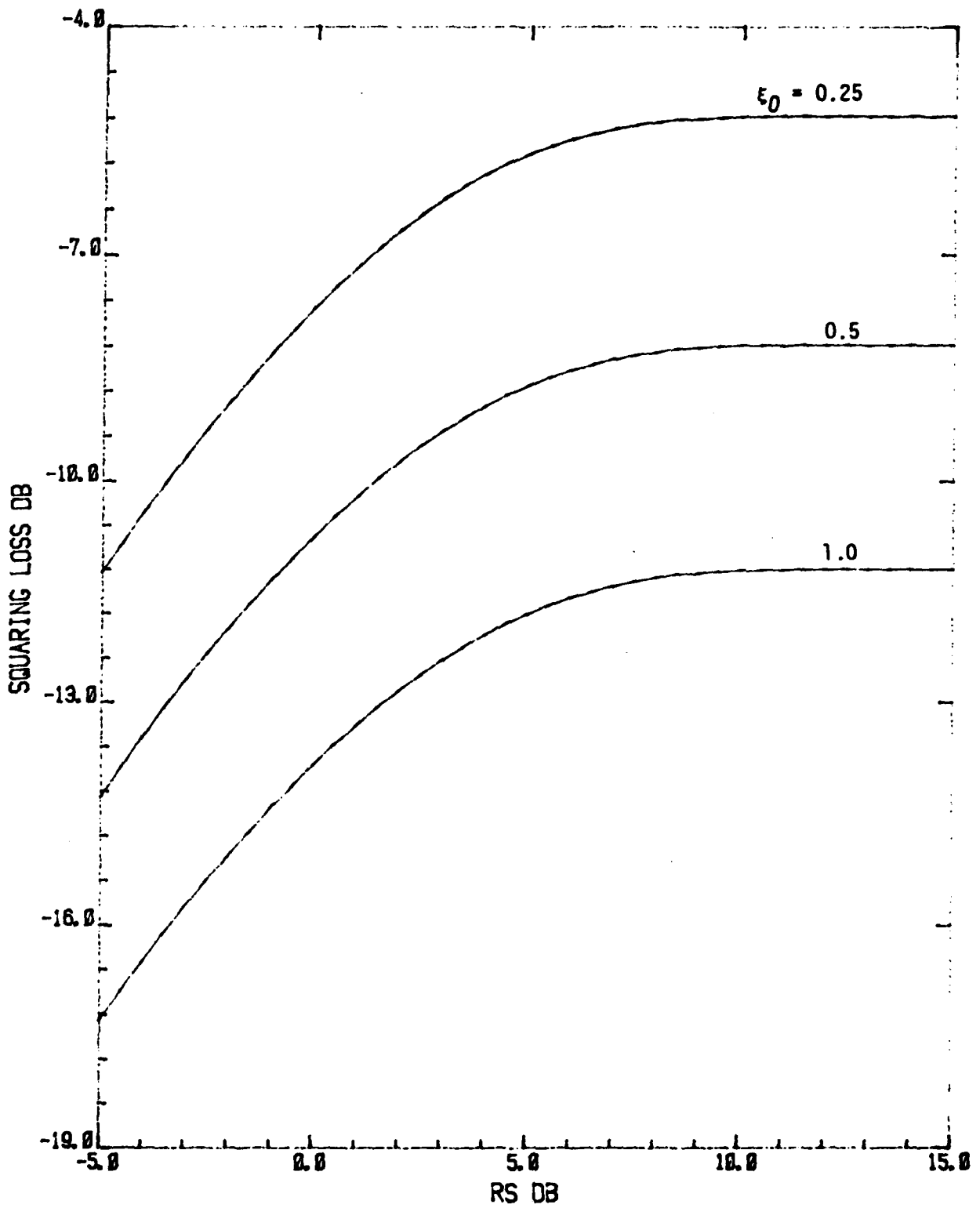


Figure 19. S_L vs R_S for DCTL Bi-Phase Format.

applications. Yet in this case, the pattern noise may not be negligible. For Bi- ϕ , the gain in optimizing f_0T is pretty small. Also, it is only of interest for narrow-band applications.

Butterworth filters of order 1 (RC filter), 2, and 3 have relatively the same performance in the small R_s region. For $R_s > 0$ dB (Bi- ϕ case), Butterworth filter of order 2 or 3 is recommended.

Manchester signaling format performs better than the NRZ signaling format for all cases of interest. It is the one to be recommended in terms of synchronization performance.

The CSSL system performs roughly the same with a DTTL with 50% window. However, in the case of DTTL, the window width can be reduced, subject to the hardware restriction.

The CSSL has the advantage of simplicity in implementation. However, it is analog in nature, some disadvantages in using analog circuits, such as drift, start up calibration, saturation, etc., need to be considered. Digital version of CSSL could be more attractive in the future.

APPENDIX A

This appendix derives the Eq. (12) in the main text. From Eq. (11) in the main text, we have

$$C(t) = \sum_{n=-\infty}^{\infty} C_n e^{j\omega_n t} \quad (\text{A.1})$$

where

$$\omega_n = \frac{2n\pi}{T}$$

$$C_n = \frac{1}{T} \int_0^T C(t) e^{-j\omega_n t} dt \quad (\text{A.2})$$

Substitute Eq. (10) into (A.2) to get

$$C_n = \frac{1}{T} \int_0^T \left[\sum_k \hat{p}(t-kT) \hat{p}(t-\alpha T-kT) + (p-q)^2 \sum_{\substack{k, i \\ i \neq k}} \hat{p}(t-iT) \hat{p}(t-\alpha T-kT) \right] e^{-j\omega_n t} dt \quad (\text{A.3})$$

By change of variable, $i = \ell+k$, in the second term of C_n , the integral can be written to

$$C_n = \frac{1}{T} \int_{-\infty}^{\infty} [\hat{p}(t) \hat{p}(t-\alpha T) + (p-q)^2 \sum_{\substack{\ell=-\infty \\ \ell \neq 0}}^{\infty} \hat{p}(t-\ell T) \hat{p}(t-\alpha T)] e^{-j\omega_n t} dt \quad (\text{A.4})$$

By using the Parseval's theorem, with $\hat{P}(\omega) = P(\omega)H(\omega)$, (A.4) can be written in the frequency domain

$$C_n = \frac{1}{2\pi T} \int_{-\infty}^{\infty} \hat{P}(\omega) \hat{P}(\omega_n - \omega) e^{-j\omega \alpha T} \left[1 + (p-q)^2 \sum_{\substack{\ell=-\infty \\ \ell \neq 0}}^{\infty} e^{-j(\omega_n - \omega)\ell T} \right] d\omega \quad (\text{A.5})$$

With the help of the Poisson sum formula,

$$\sum_{k=-\infty}^{\infty} h(kT)e^{-jk\omega T} = \frac{1}{T} \sum_{k=-\infty}^{\infty} H\left(\omega - \frac{2\pi k}{T}\right) \quad (\text{A.6})$$

(A.5) can be written as Eq. (12) in the main text.

APPENDIX B

This appendix evaluates $S_m(\omega)$ in Eq. (24). From Eq. (2),

$$m(t) = \sum_k a_k p(t-kT) \quad (B.1)$$

$m(t)$ is a cyclostationary process, its spectrum is defined to be

$$\begin{aligned} S_m(\omega) &\triangleq \underline{E}\{\overline{\langle m(t)m(t+\tau) \rangle}\} \\ &= \underline{E}\left\{\sum_k p(t-kT)p(t+\tau-kT) + (p-q)^2 \sum_{\substack{n \neq k \\ n, k}} p(t-nT)p(t+\tau-kT)\right\} \quad (B.2) \end{aligned}$$

Consider the first term

$$\begin{aligned} &\underline{E}\left\{\sum_k p(t-kT)p(t+\tau-kT)\right\} \\ &= \underline{E}\left\{\sum_k \frac{1}{T} \int_0^T p(t-kT)p(t+\tau-kT) dt\right\} \\ &= \frac{1}{T} \int_{-\infty}^{\infty} \int_{-\infty}^{\infty} p(t)p(t+\tau)e^{-j\omega\tau} dt d\tau \\ &= \frac{1}{T} \int_{-\infty}^{\infty} p(t) \int_{-\infty}^{\infty} p(t+\tau)e^{-j\omega\tau} d\tau dt \\ &= \frac{1}{T} P(\omega) \int_{-\infty}^{\infty} p(t)e^{j\omega t} dt \\ &= \frac{1}{T} P(\omega)P(-\omega) \quad (B.3) \end{aligned}$$

Similarly, for the second term

$$\begin{aligned}
& \underline{E}\left\{\left\langle \sum_{\substack{n \neq k \\ n \neq k}} p(t-nT)p(t+\tau-kT) \right\rangle\right\} \\
&= \underline{E}\left\{\sum_{\ell \neq 0} \sum_k \frac{1}{T} \int_0^T p(t-\ell T-kT)p(t+\tau-kT)dt\right\} \\
&= \underline{E}\left\{\frac{1}{T} \sum_{\ell \neq 0} \int_{-\infty}^{\infty} p(t-\ell T)p(t+\tau)dt\right\} \\
&= \frac{1}{T} \sum_{\ell \neq 0} \int_{-\infty}^{\infty} p(t-\ell T) \int_{-\infty}^{\infty} p(t+\tau)e^{-j\omega\tau}d\tau dt \\
&= \frac{1}{T} P(\omega)P(-\omega) \sum_{\ell \neq 0} e^{j\omega\ell T} \\
&= \frac{1}{T} P(\omega)P(-\omega) \left[-1 + \frac{2\pi}{T} \sum_{\ell=-\infty}^{\infty} \delta\left(\omega + \frac{2\pi\ell}{T}\right)\right] \tag{B.4}
\end{aligned}$$

Therefore,

$$S_m(\omega) = \frac{1}{T} P(\omega)P(-\omega) \left[4pq + \frac{2\pi}{T} (p-q)^2 \sum_{\ell=-\infty}^{\infty} \delta\left(\omega + \frac{2\pi\ell}{T}\right)\right] \tag{B.5}$$

APPENDIX C

This appendix presents a brief derivation of the S_L for DTTL. The S_L can be determined given the loop S-curve $g(\lambda)$ and the equivalent noise spectrum $S(\omega, \lambda)$ [1]. By using a Gaussian approximation for the probability density function of λ , the squaring loss is found to be

$$S_L \approx \frac{1}{(2n\pi)^2 \rho \sigma_\lambda^2} = \frac{2[g'_n(0)]^2}{(2n\pi)^2 \epsilon_0 h(0)} \quad (C.1)$$

where $g'_n(0)$ is the derivative of the normalized S-curve at $\lambda = 0$, $h(0)$ is the normalized noise spectrum at $\lambda = 0$, and n is set to be 1 for NRZ and 2 for biphasic format.

For NRZ format [1]

$$g_n(\lambda) = \frac{1}{4} \left[\left(\lambda - \frac{\epsilon_0}{2} \right) \text{erf}(\sqrt{R_s}) + \left(3\lambda + \frac{\epsilon_0}{2} \right) \text{erf}(\sqrt{R_s}(1-2\lambda)) \right]; \quad 0 < \lambda < \frac{\epsilon_0}{2} \quad (C.2)$$

$$g'_n(0) = \frac{1}{2} \left[2 \text{erf}(\sqrt{R_s}) - \epsilon_0 \frac{\sqrt{R_s}}{\pi} e^{-R_s} \right] \quad (C.3)$$

$$h(0) = 1 + \frac{1}{2} R_s \epsilon_0 - \frac{\epsilon_0}{\pi} e^{-2R_s} - \frac{R_s \epsilon_0}{2} \text{erf}^2(\sqrt{R_s}) - \frac{\sqrt{R_s}}{\pi} \epsilon_0 e^{-R_s} \text{erf}(\sqrt{R_s}) \quad (C.4)$$

For bi-phase format, $g_n(\lambda)$ and $h(0)$ can be found by the similar method [7] with the period to be tracked replaced by $T/2$. With the help of Fig. C.1 and Tables C.1, C.2, and C.3, we have

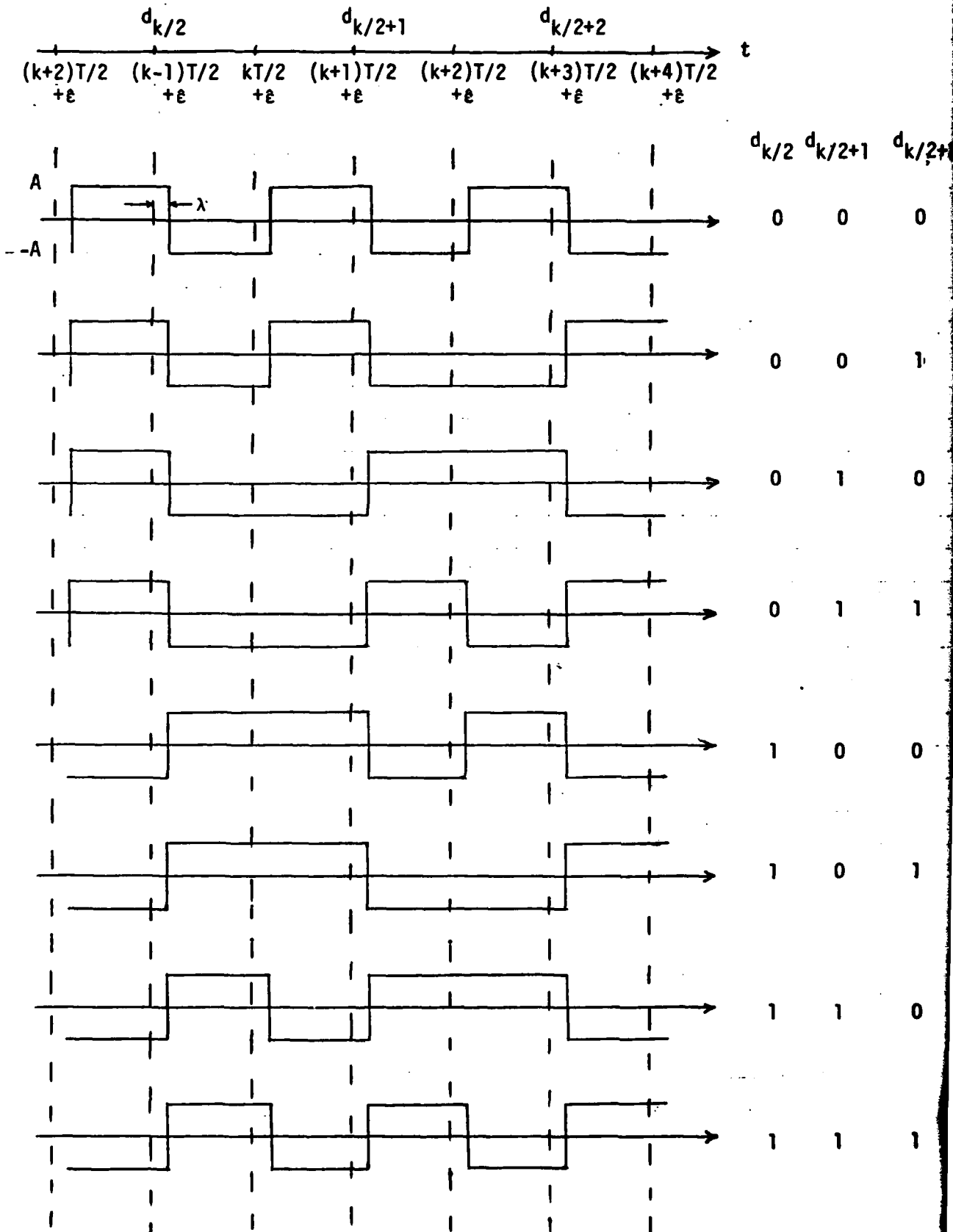


Figure C.1. Bi-Phase Signal $S(t)$ for Different Data Patterns.

Table C.1. Definition of $x_{(i)}$ and $y_{(i)}$.

| | | |
|---|------------------------|---|
| 1 | $x_{(i)}; \lambda > 0$ | $y_{(i)}; 0 < \lambda < \frac{\epsilon_0}{2}$ |
| 1 | $1 - 4\lambda$ | 4λ |
| 2 | 1 | ϵ_0 |

Table C.2. Values of x_k, y_k for Different Data Patterns, Unshifted Case.

| $d_{k/2}$ | $d_{k/2+1}$ | x_k | x_{k+1} | x_{k+2} | y_k | y_{k+1} |
|-----------|-------------|---------|-----------|-----------|--------|-----------|
| 0 | 0 | $-x(1)$ | x_1^* | $-x_1$ | $-y_1$ | y_1 |
| 0 | 1 | $-x(1)$ | $-x_2$ | x_1 | $-y_2$ | $-y_1$ |
| 1 | 0 | $x(1)$ | x_2 | $-x_1$ | y_2 | y_1 |
| 1 | 1 | $x(1)$ | $-x_1$ | x_1 | y_1 | $-y_1$ |

* For convenience, the bracket in the subscript is neglected. The entries in the Tables C.2 and C.3 should look like the first column.

Table C.3. Values of x_k, y_k for Different Data Patterns, Shifted Case.

| $d_{k/2}$ | $d_{k/2+1}$ | $d_{k/2+2}$ | x_k | x_{k+1} | x_{k+2} | y_k | y_{k+1} |
|-----------|-------------|-------------|--------|-----------|-----------|--------|-----------|
| 0 | 0 | 0 | x_1 | $-x_1$ | x_1 | y_1 | $-y_1$ |
| 0 | 0 | 1 | x_1 | $-x_1$ | $-x_2$ | y_1 | $-y_2$ |
| 0 | 1 | 0 | $-x_2$ | x_1 | x_2 | $-y_1$ | y_2 |
| 0 | 1 | 1 | $-x_2$ | x_1 | $-x_1$ | $-y_1$ | y_1 |
| 1 | 0 | 0 | x_2 | $-x_1$ | x_1 | y_1 | $-y_1$ |
| 1 | 0 | 1 | x_2 | $-x_1$ | $-x_2$ | y_1 | $-y_2$ |
| 1 | 1 | 0 | $-x_1$ | x_1 | x_2 | $-y_1$ | y_2 |
| 1 | 1 | 1 | $-x_1$ | x_1 | $-x_1$ | $-y_1$ | y_1 |

$$g_n(\lambda) = \frac{1}{3} E_s \frac{Y_k}{2} [\operatorname{erf}(\sqrt{\frac{R_s}{2}} x_k) - \operatorname{erf}(\sqrt{\frac{R_s}{2}} x_{k+1})] + \frac{E_0}{\sqrt{8\pi R_s}} [\exp(-\frac{R_s x_k^2}{2}) - \exp(-\frac{R_s x_{k+1}^2}{2})] \quad (C.5)$$

where

$$x_k \triangleq \frac{1}{AT/2} \int_{(k-1)\frac{T}{2} + \hat{\epsilon}}^{k\frac{T}{2} + \hat{\epsilon}} s(t) dt$$

$$y_k \triangleq \int_{(k-\frac{E_0}{2})\frac{T}{2} + \hat{\epsilon}}^{(k+\frac{E_0}{2})\frac{T}{2} + \hat{\epsilon}} s(t) dt$$

and their values for different data patterns are given in Tables C.2 and C.3. The expectation is averaged over the signal patterns. Half of the signal pattern is shown in Fig. C.1 and the other half is the same as Fig. C.1 except $T/2$ shifted to the right. The normalized equivalent noise spectrum at $\lambda = 0$ is found by

$$h(0) = \frac{2}{3} [Q(0|\lambda) + 2Q(1|\lambda)] \quad (C.6)$$

where

$$Q(0|\lambda) = E_s \left\{ \left[1 + \frac{R_s y_k^2}{E_0} \right] \left[1 - \operatorname{erf}(\sqrt{\frac{R_s}{2}} x_k) \operatorname{erf}(\sqrt{\frac{R_s}{2}} x_{k+1}) \right] - \sqrt{\frac{2R_s}{\pi}} \left[y_k - \frac{1}{4} E_0 x_k \right] \exp(-\frac{R_s}{2} x_k^2) \operatorname{erf}(\sqrt{\frac{R_s}{2}} x_{k+1}) - \sqrt{\frac{2R_s}{\pi}} \left[y_k - \frac{1}{4} E_0 x_{k+1} \right] \exp(-\frac{R_s}{2} x_{k+1}^2) \operatorname{erf}(\sqrt{\frac{R_s}{2}} x_k) - \frac{E_0}{\pi} \exp(-\frac{R_s}{2} x_k^2) \exp(-\frac{R_s}{2} x_{k+1}^2) \right\} \quad (C.7)$$

and

$$\begin{aligned}
Q(1|\lambda) = & E_s \left\{ \frac{R_s}{2E_0} y_k y_{k+1} [\operatorname{erf}(\sqrt{\frac{R_s}{2}} x_{k+1}) \operatorname{erf}(\sqrt{\frac{R_s}{2}} x_{k+2}) \right. \\
& + \operatorname{erf}(\sqrt{\frac{R_s}{2}} x_k) \operatorname{erf}(\sqrt{\frac{R_s}{2}} x_{k+1}) - \operatorname{erf}(\sqrt{\frac{R_s}{2}} x_k) \operatorname{erf}(\sqrt{\frac{R_s}{2}} x_{k+2}) - 1] \\
& + \sqrt{\frac{R_s}{8\pi}} y_k [\exp(-\frac{R_s}{2} x_{k+1}^2) (\operatorname{erf}(\sqrt{\frac{R_s}{2}} x_{k+2}) + \operatorname{erf}(\sqrt{\frac{R_s}{2}} x_k)) \\
& + \exp(-\frac{R_s}{2} x_{k+2}^2) (\operatorname{erf}(\sqrt{\frac{R_s}{2}} x_{k+1}) - \operatorname{erf}(\sqrt{\frac{R_s}{2}} x_k))] \\
& + \sqrt{\frac{R_s}{4\pi}} y_{k+1} [\exp(-\frac{R_s}{2} x_{k+1}^2) (\operatorname{erf}(\sqrt{\frac{R_s}{2}} x_{k+2}) + \operatorname{erf}(\sqrt{\frac{R_s}{2}} x_k)) \\
& - \exp(-\frac{R_s}{2} x_k^2) (\operatorname{erf}(\sqrt{\frac{R_s}{2}} x_{k+2}) - \operatorname{erf}(\sqrt{\frac{R_s}{2}} x_{k+1}))] \\
& + \frac{E_0}{4\pi} \exp(-\frac{R_s}{2} x_k^2) [\exp(-\frac{R_s}{2} x_{k+1}^2) - \exp(-\frac{R_s}{2} x_{k+2}^2)] \\
& \left. + \frac{E_0}{4\pi} \exp(-\frac{R_s}{2} x_{k+1}^2) [\exp(-\frac{R_s}{2} x_{k+2}^2) - \exp(-\frac{R_s}{2} x_{k+1}^2)] \right\}
\end{aligned}$$

(C.8)

REFERENCES

1. W. C. Lindsey and M. K. Simon, Telecommunication Systems Engineering, Prentice-Hall, Inc., Englewood Cliffs, NJ, 1973.
2. J. J. Spilker, Jr., Digital Communications by Satellite, Prentice-Hall, Inc., Englewood Cliffs, NJ, 1977.
3. J. K. Holmes, "Tracking Performance of the Filter and Square Bit Synchronizer," IEEE Trans. Comm., Vol. COM-28, pp. 1154-1158, Aug. 1980.
4. R. D. McCallister and M. K. Simon, "Cross-Spectrum Symbol Synchronization," Proceedings ICC'81, Vol. pp. 34.3.1-34.3.6.
5. W. C. Lindsey, Synchronization Systems in Communication and Control, Prentice-Hall, Inc., Englewood Cliffs, NJ, 1972.
6. F. M. Gardner, "Self-Noise in Synchronizers," IEEE Trans. Comm., Vol. COM-28, pp. 1159-1163, Aug. 1980.
7. M. K. Simon, "An Analysis of the Steady State Phase Noise Performance of a Digital Data-Transition Tracking Loop," Jet Propulsion Laboratory, Pasadena, CA, Nov. 1968.